iScience

CellPress

Article

A Pivotal Genetic Program Controlled by Thyroid Hormone during the Maturation of GABAergic Neurons

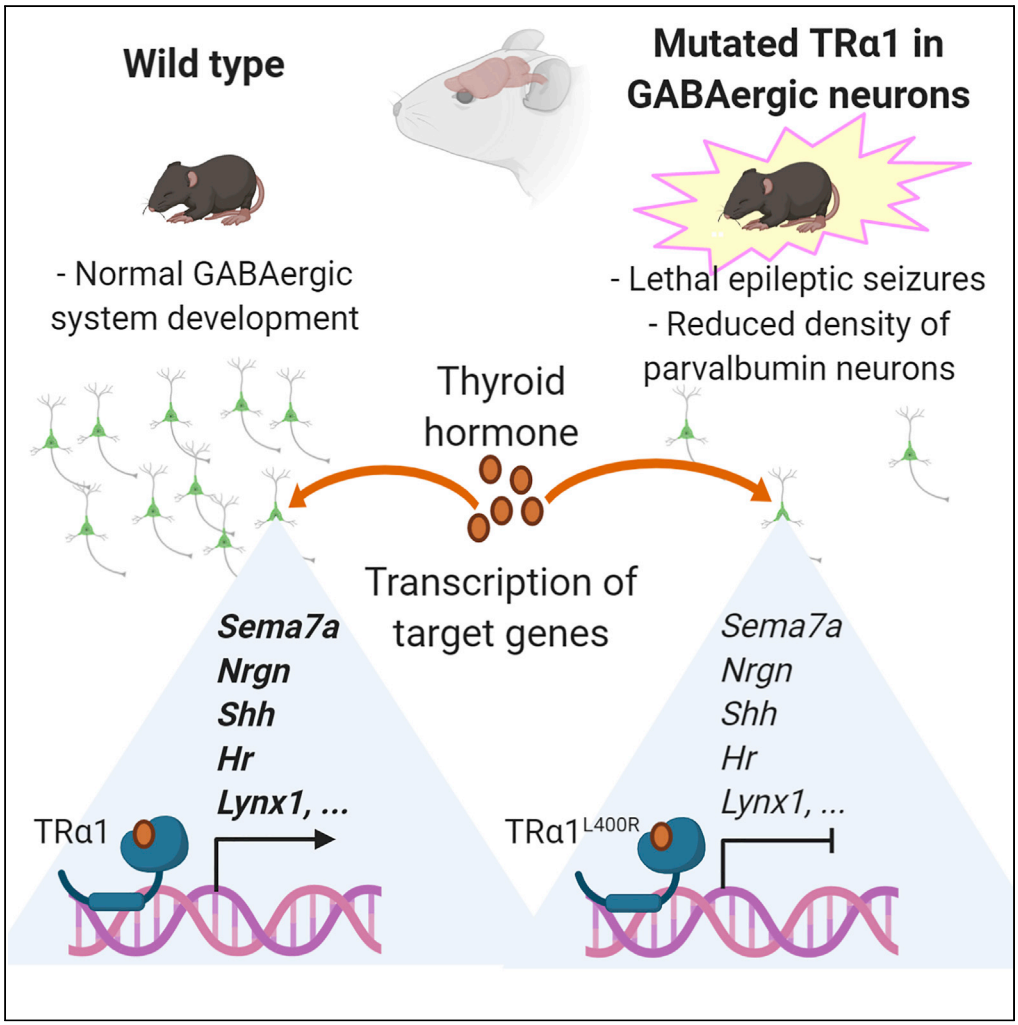

Sabine Richard, Romain Guyot, Martin Rey-Millet, Margaux Prieux, Suzy Markossian, Denise Aubert, Frédéric Flamant

sabine.richard@ens-lyon.fr

HIGHLIGHTS

GABAergic neurons are a direct target of thyroid hormone in the developing brain

Impaired TH/TRα1 signaling severely impairs the development of GABAergic neurons

GABAergic-specific genes directly targeted by TH/TRα1 signaling have been listed

A defect in the GABAergic system is expected in patients with a *THRA* mutation

DATA AND CODE AVAILABILITY

GSE143933

Richard et al., iScience *23*, 100899
March 27, 2020
https://doi.org/10.1016/j.isci.2020.100899

iScience

CellPress

Article

A Pivotal Genetic Program Controlled by Thyroid Hormone during the Maturation of GABAergic Neurons

Sabine Richard,[1,2,*] Romain Guyot,[1] Martin Rey-Millet,[1] Margaux Prieux,[1] Suzy Markossian,[1] Denise Aubert,[1] and Frédéric Flamant[1]

SUMMARY

Mammalian brain development critically depends on proper thyroid hormone signaling, via the TRα1 nuclear receptor. The downstream mechanisms by which TRα1 impacts brain development are currently unknown. In order to investigate these mechanisms, we used mouse genetics to induce the expression of a dominant-negative mutation of TRα1 specifically in GABAergic neurons, the main inhibitory neurons in the brain. This triggered post-natal epileptic seizures and a profound impairment of GABAergic neuron maturation in several brain regions. Analysis of the transcriptome and TRα1 cistrome in the striatum allowed us to identify a small set of genes, the transcription of which is upregulated by TRα1 in GABAergic neurons and which probably plays an important role during post-natal maturation of the brain. Thus, our results point to GABAergic neurons as direct targets of thyroid hormone during brain development and suggest that many defects seen in hypothyroid brains may be secondary to GABAergic neuron malfunction.

INTRODUCTION

Thyroid hormones (TH, including thyroxine, or T4, and 3,3′,5-triiodo-L-thyronine, or T3, its active metabolite) exert a broad influence on neurodevelopment. If untreated soon after birth, congenital hypothyroidism, i.e. early TH deficiency, affects brain development and a number of cognitive functions (Rovet, 2014). Severe cases display mental retardation, autism spectrum disorders (ASD), and epilepsy (Fetene et al., 2017). TH mainly acts by binding to nuclear receptors called TRα1, TRβ1, and TRβ2, which are encoded by the *THRA* and *THRB* genes (*Thra* and *Thrb* in mice, formerly *TRα* and *TRβ*). These receptors form heterodimers with other nuclear receptors, the retinoid X receptors (RXRs), and bind chromatin at specific locations (thyroid hormone response elements), acting as TH-dependent transcription activators of neighboring genes. In the developing brain, the predominant type of receptor is TRα1 (Bradley et al., 1989). Accordingly, *THRA* germline mutations, which have currently been reported in only 45 patients, cause a syndrome named RTHα (resistance to thyroid hormone due to *THRA* mutations), resembling congenital hypothyroidism, with mental retardation and a high occurrence of ASD and epilepsy (van Gucht et al., 2017).

Cellular alterations caused by early TH deficiency or germline mutations have been extensively studied in rodents. Many neurodevelopmental processes depend on proper TH signaling, and virtually all glial and neuronal cell populations are affected by TH deficiency (Berbel et al., 2014; Bernal et al., 2003). However, in the mouse cerebellum, we have previously found that, although *Thra* expression is ubiquitous in this brain region, only a subset of cell types displayed a direct, cell-autonomous, response to TH (Fauquier et al., 2014). More specifically, Cre/*loxP* technology, used to express a dominant-negative variant of TRα1 (TRα1^{L400R}), has provided genetic evidence that the cell-autonomous influence of TRα1 is limited to astrocytes and GABAergic neurons (Fauquier et al., 2014). By altering the differentiation of GABAergic neurons, TRα1^{L400R} prevented the secretion of several growth factors and neurotrophins. This indirectly altered the proliferation and differentiation of granule cells and oligodendrocytes (Picou et al., 2012, 2014). Therefore, GABAergic neurons occupy a pivotal position during cerebellum development, amplifying the initial TH signal. This allows TH to synchronize cellular interactions and the maturation of neuronal networks during the first post-natal weeks (Flamant et al., 2017). As defects in TH signaling are known to alter GABAergic neurons outside the cerebellum (Berbel et al., 1996; Harder et al., 2018; Wallis et al., 2008), we asked whether the direct role of TH in GABAergic neurons, initially observed in the cerebellum, could be generalized to other brain regions.

[1]Univ Lyon, ENS de Lyon, INRAE, CNRS, Institut de Génomique Fonctionnelle de Lyon, 69364 Lyon, France

[2]Lead Contact

*Correspondence: sabine.richard@ens-lyon.fr

https://doi.org/10.1016/j.isci.2020.100899

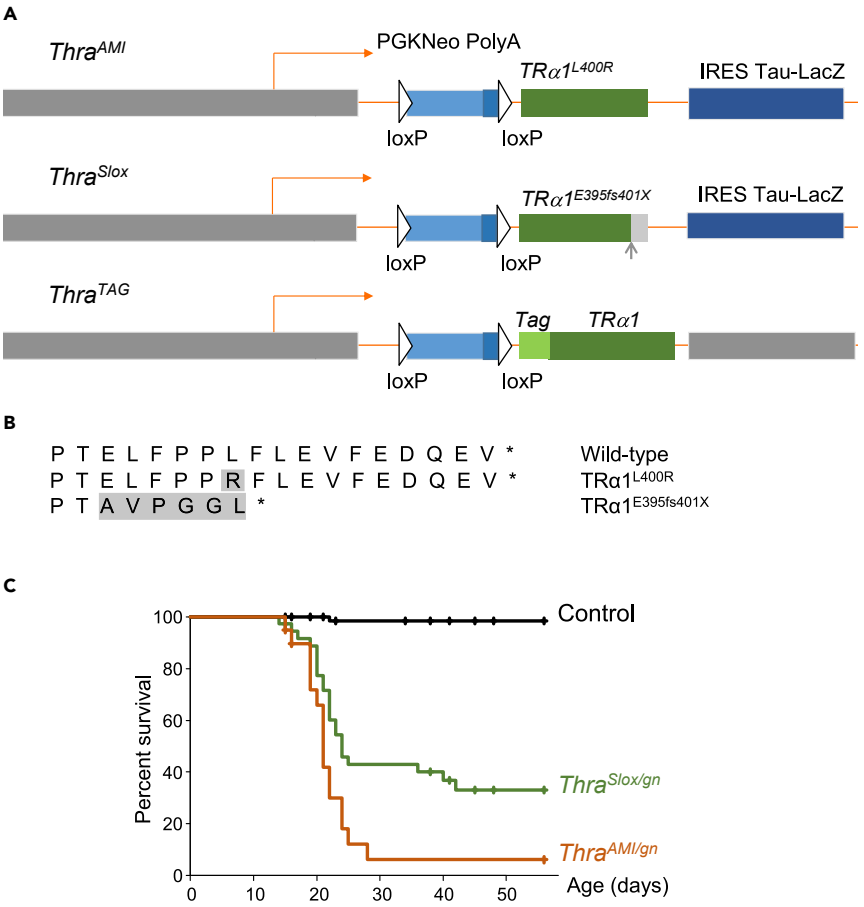

Figure 1. *Thra* Alleles and Survival Curves

(A) Schematic representation of *Thra* alleles in $Thra^{AMI}$, $Thra^{Slox}$ and $Thra^{TAG}$ mice. In all 3 alleles, the coding sequence is preceded with a floxed stop cassette (PGKNeo Poly(A). The intronless structure eliminates alternate splicing and internal promoter and thus prevents the production of TRα2, TRΔα1, and TRΔα2 non-receptor protein. The dispensable IRES Tau-lacZ reporter part was not included in the $Thra^{TAG}$ construct.

(B) C-terminal amino acid sequence of *Thra* gene products used in the present study, starting from AA393. Shaded amino acids differ from wild-type TRα1. $Thra^{AMI}$ mutation results in a single amino acid substitution within TRα1 helix 12. $Thra^{Slox}$ mutation is a deletion resulting in a +1 frameshift, leading to elimination of helix 12, as in several RTHα patients.

(C) Survival curves of mice expressing a mutated TRα1 in GABAergic neurons (green and red lines) and of control littermates (black line).

See also Figures S1–S3 and Videos S1 and S2.

In the present study, we used the same genetic strategy to block TH response in the entire GABAergic lineage by expressing $TR\alpha1^{L400R}$ from early developmental stages specifically in GABAergic neurons in all brain areas. This had dramatic neurodevelopmental consequences on the development of the GABAergic system and caused lethal epileptic seizures. Genome-wide analyses allowed us to pinpoint the genetic defects induced by the mutation and to identify a small set of genes activated by TH in GABAergic neurons. These genes are likely to play a key role in the neurodevelopmental function of TH.

RESULTS

Mouse Models Designed to Target TRα1 in GABAergic Neurons

We generated new mouse models by combining existing and novel "floxed" *Thra* alleles with the *Gad2Cre* transgene (Figure 1A). This transgene drives the expression of Cre recombinase in all GABAergic neurons and their progenitors from an early prenatal stage (around E12.5) (Taniguchi et al., 2011). In the context of the modified *Thra* alleles used in the present study, Cre recombinase eliminates a transcriptional stop cassette and triggers the expression of TRα1 variants. The $Thra^{AMI}$ allele (formerly $TR\alpha^{AMI}$) (Quignodon

et al., 2007) encodes TRα1^{L400R} (Figure 1B), which exerts a permanent transcriptional repression on target genes, even in the presence of TH. This is due to its inability to recruit transcription coactivators, which normally interact with the C-terminal helix (AA 398-407) of TRα1, and permanent interaction with transcription corepressors (Figure S1). This allelic design, which eliminates alternate splicing, increases the expression of the mutant receptor over that of the wild-type receptor, as shown by comparing peak surfaces after Sanger sequencing: in the striatum of *Thra*$^{AMI/gn}$ mice, the *Thra*^{AMI} allele represents 65 ± 4% of all *Thra* transcripts (mean ± standard deviation, n = 4; see also (Markossian et al., 2018)). This ensures a complete inhibition of TH response in heterozygous cells (Markossian et al., 2018). As complete deprivation of TH (Mansouri et al., 1998), ubiquitous expression of TRα1^{L400R} results in the death of heterozygous mice 2–3 weeks after birth (Quignodon et al., 2007). The second modified *Thra* allele, named *Thra*^{Slox}, differs from *Thra*^{AMI} only by an additional frameshift mutation, which eliminates the C-terminal helix of TRα1 (Markossian et al., 2018). As for *Thra*^{AMI}, expression of the *Thra*^{Slox} allele exceeds that of the wild-type *Thra* allele: in the striatum of *Thra*$^{Slox/gn}$ mice, the *Thra*^{Slox} allele represents 59 ± 1% of all *Thra* transcripts (mean ± standard deviation, n = 6). The *Thra*^{Slox} allele encodes TRα1^{E395fs401X} (Figure 1B), which is nearly identical to a pathological variant found in a patient (van Mullem et al., 2012, 2014). TRα1^{E395fs401X} is expected to be functionally equivalent to TRα1^{L400R} and behaves similarly in *in vitro* assays (Markossian et al., 2018). The third modified *Thra* allele used in the present study is *Thra*^{TAG}, a novel construct that encodes a functional receptor, TRα1^{TAG}, with a fragment of protein G at its N-terminus (Burckstummer et al., 2006). This tag has a high affinity for IgGs, which makes it suitable to address chromatin occupancy (Chatonnet et al., 2013). Transient expression assays show that the N-terminal GS tag does not impair the transactivation capacity of TRα1 (Figure S2). Double heterozygous mice, combining the presence of *GADad2Cre* and of a modified *Thra* allele, express TRα1^{L400R}, TRα1^{E395fs401X}, or TRα1^{TAG} in the GABAergic cell lineage only. They will be respectively designated as *Thra*$^{AMI/gn}$, *Thra*$^{Slox/gn}$, and *Thra*$^{TAG/gn}$ in the following,*/gn* being used to indicate that the modified *Thra* alleles were expressed specifically in GABAergic neurons. In all phenotyping experiments, littermates carrying only *Thra*^{AMI}, *Thra*^{Slox}, or *GAD2Cre* were used as controls.

Post-natal Lethality Caused by Thra Mutations in GABAergic Neurons

Born at the expected frequency, *Thra*$^{AMI/gn}$ mice did not usually survive beyond the third post-natal week (Figure 1C). Video recording of litters in their home cage indicated that most mice started to display epileptic seizures a few days before death. Occasionally, sudden death was observed at the end of a seizure. In most cases, seizures impeded maternal care and this likely precipitated the death of the pups (Videos S1 and S2). Although lethality was also observed in *Thra*$^{Slox/gn}$ mice (Figure 1C), about one-third of these mice survived into adulthood. Adult *Thra*$^{Slox/gn}$ mice did not display any obvious epileptic seizure anymore. However, their locomotor behavior was significantly altered, as evidenced in an open-field test (Figure S3). These observations show that, although the two mutations are expected to be equivalent, TRα1^{E395fs401X} is less detrimental than TRα1^{L400R}.

A Global Impairment in the Differentiation of GABAergic Neurons

In order to label neurons of the GABAergic lineage in a generic way, we combined the *Thra*^{AMI} and *Gad2-Cre* alleles with the *Rosa-tdTomato* transgene, which enabled to trace the cells in which *Cre/loxP* recombination had taken place. The density of tdTomato + cells was not reduced in *Thra*$^{AMI/gn}$ *Rosa-tdTomato* mice, arguing against a possible alteration in the proliferation, migration, or survival of GABAergic neuron progenitors. In the hippocampus, notably in the dentate gyrus, the number of tdTomato + cells was even increased (Figure 2).

We used immunohistochemistry to detect alterations of GABAergic neuron differentiation at postnatal day 14 (PND14) in various brain areas (quantitative data in Tables 1 and S1). Parvalbumin (PV) immunostaining, which labels major populations of GABAergic neurons in several brain areas (DeFelipe et al., 2013), revealed a defect in Purkinje cell arborization and a deficit in basket and stellate GABAergic interneurons in *Thra*$^{AMI/gn}$ cerebellum as expected from previous data (Fauquier et al., 2011; Markossian et al., 2018) (Figure S4). A drastic reduction in the density of PV + neurons (90%–95% reduction relative to controls) was also visible in the hippocampus, cortex, and striatum of *Thra*$^{AMI/gn}$ mice (Figure 3A). As a complement to PV labeling, we used *Wisteria floribunda* lectin (WFA) to label perineuronal nets, as it has been previously reported that a reduction in PV + neuron numbers may be accompanied by a persistence of these extracellular matrix structures (Filice et al., 2016). In *Thra*$^{AMI/gn}$ mice, WFA labeling was drastically reduced compared with that of control mice, but perineuronal nets were observed around PV-negative cell bodies

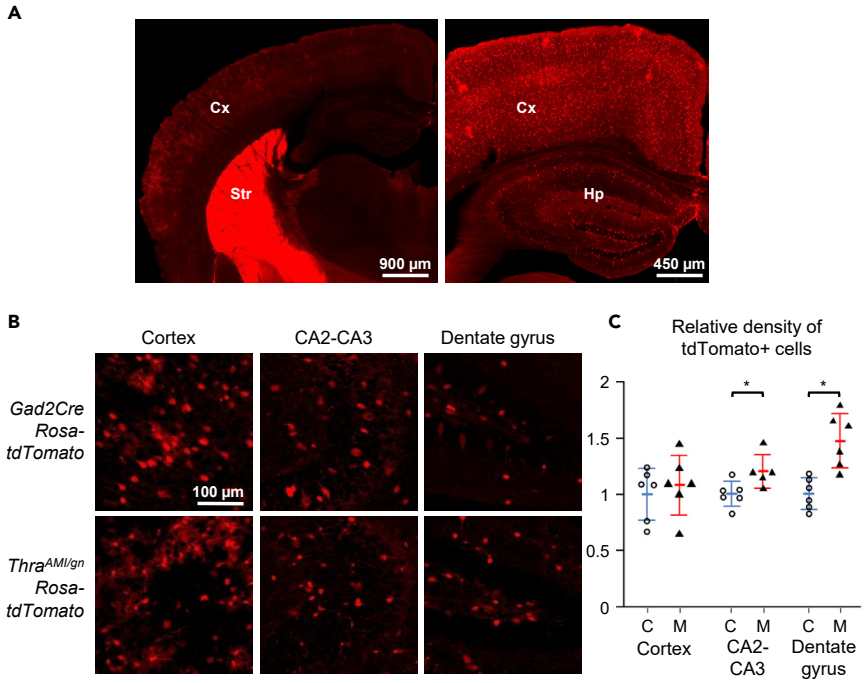

Figure 2. Expression of the tdTomato Fluorescent Protein in *TRα*$^{AMI/gn}$ *Rosa-tdTomato* and Control Littermates at PND14

(A) Low-magnification images illustrating the relative fluorescence intensity in the cortex (Cx), striatum (Str), and hippocampus (Hp) in *GAD2Cre Rosa-tdTomato* mice.

(B) Representative images allowing to compare the density of tdTomato positive cells in selected brain regions in *Thra*$^{AMI/gn}$ *Rosa-tdTomato* and control littermates (*GAD2Cre Rosa-tdTomato*).

(C) Relative density of tdTomato + cells in *Thra*$^{AMI/gn}$ *Rosa-tdTomato* ("M" in the graph stands for mutants, filled triangles; red lines for the mean and standard deviation) and control littermates ("C", empty circles; blue lines for the mean and standard deviation) at PND14. *$p < 0.05$.

(Figure S5), suggesting that absence of PV labeling was not necessarily a sign of PV neuron loss. We also used antibodies directed against calretinin (CR), somatostatin (SST), and neuropeptide Y (NPY) to label other key populations of GABAergic neurons (Kepecs and Fishell, 2014). All GABAergic neuron subtypes investigated were affected but in a rather complex pattern. The density of CR + neurons was increased in the cortex and CA2-CA3 area of the hippocampus. In the hippocampal dentate gyrus, where CR + neurons are normally concentrated in the granular cell layer, the limits of this layer were ill-defined and CR + neurons spread into the molecular and polymorph layers (Figure 3B). The density of SST + neurons was also augmented in hippocampal dentate gyrus but not significantly altered in the cortex or striatum (Figure 4A). The density of NPY + neurons was significantly reduced in the cortex, but not in the striatum and hippocampus, where, by contrast, NPY immunoreactivity of the fibers increased (Figures 4B and Table 1).

Most of the above-mentioned immunohistochemistry experiments were also carried out in *Thra*$^{Slox/gn}$ mice at PND14. In all instances, the defects observed in GABAergic neuron populations were the same as in *Thra*$^{AMI/gn}$ mice (details in Table S1 and Figure S6). In the surviving *Thra*$^{Slox/gn}$ adult mice, PV and NPY immunohistochemistry indicated that the differentiation of neurons expressing these markers was not only delayed, but permanently impaired (Figure S7 and Table S1). Taken together, these data indicate that expressing a mutant TRα1 alters the late steps of development of GABAergic neurons, reducing the numbers of PV+ and NPY + cells in some brain areas, while favoring an expansion of the SST+ and CR + cell populations. In the hippocampus, this is accompanied by subtle morphological alterations.

Changes in Gene Expression Caused by TRα1^{L400R} in GABAergic Neurons

Because the impairment in GABAergic neuron differentiation does not appear to be restricted to a specific brain area or a specific neuronal GABAergic subpopulation, we hypothesized that a general

		Cortex		Hippocampus (DG)		Hippocampus (CA)		Striatum	
		Control	*Thra*$^{AMI/gn}$	Control	*Thra*$^{AMI/gn}$	Control	*Thra*$^{AMI/gn}$	Control	*Thra*$^{AMI/gn}$
Parvalbumin neuronal density	Mean	1.00	0.05[a]	1.00	0.05[a]	1.00	0.33[a]	1.00	0.10[a]
	SD	0.14	0.01	0.50	0.13	0.34	0.21	0.48	0.15
	n	11	10	11	12	11	10	10	8
Neuropeptide Y neuronal density	Mean	1.00	0.58[a]	1.00	0.92	ND	ND	1.00	1.07
	SD	0.00	0.11	0.00	0.06	ND	ND	0.11	0.20
	n	5	6	3	3	ND	ND	5	6
Neuropeptide Y fluorescence intensity	Mean	ND	ND	1.00	1.23[a]	ND	ND	1.00	1.31[a]
	SD	ND	ND	0.00	0.08	ND	ND	0.06	0.25
	n	ND	ND	3	3	ND	ND	6	6
Calretinin neuronal density	Mean	1.00	0.75	ND	ND	1.00	4.90[a]	ND	ND
	SD	0.12	0.54	ND	ND	0.41	4.10	ND	ND
	n	5	4	ND	ND	5	4	ND	ND
Somatostatin neuronal density	Mean	1.00	1.12	1.00	2.55[a]	1.00	1.08	1.00	1.16
	SD	0.02	0.31	0.14	0.66	0.13	0.29	0.03	0.19
	n	6	5	6	5	6	5	6	5

Table 1. Relative Abundance of Several GABAergic Neuron Subtypes in *Thra*$^{AMI/gn}$, Compared with Control, Mouse Brains at PND14, as Evidenced by Immunohistochemistry

See also Table S1.

[a]Significantly different from control ($p < 0.05$).

mechanism might underlie the involvement of TH signaling in the terminal maturation of GABAergic neurons. In order to decipher this mechanism and identify the TRα1 target genes in GABAergic neurons, we first compared the transcriptome of the cortex in *Thra*$^{AMI/gn}$ and control littermates at two different post-natal stages, PND7 and PND14, where we previously found clear histological alterations. Differential gene expression analysis pointed out a set of 58 genes whose expression was deregulated in *Thra*$^{AMI/gn}$ mouse cortex, compared with age-matched control mice. Clustering analysis outlined contrasting patterns of regulations (Figure S8). Exploring available single-cell RNAseq data (https://singlecell.broadinstitute.org) obtained from adult visual cortex (Tasic et al., 2016) suggests that a large part of the observed variations reflect the alterations in neuronal maturation already revealed by immunohistochemistry. For example, many downregulated genes are preferentially expressed in PV + neurons (*Akr1c18, Dusp10, Eya4, Flywch2, Me3, Ntn4, Pcp4L1, Ppargc1a, Pvalb, Stac2, Syt2*) whereas most overexpressed genes are preferentially expressed in SST+ and/or VIP + GABAergic interneurons (*Calb1, Cxcl14, Hap1, Klhl14, Pcdh8, Prox1, Rbp4, Rxfp3, Sema3c, Sst, Tac2, Zcchc12*). Interestingly, the analysis also revealed an upregulation of *Thra* at PND7 in control mice, which was absent in mutant mice. However, we expected a larger set of differentially expressed genes on the basis of previous *in vitro* analysis (Gil-Ibanez et al., 2014). This probably results from the relatively low representation of GABAergic neurons among cortical cells. We thus decided to focus our investigation on the striatum, where the high abundance of GABAergic neurons, mainly spiny projection neurons, facilitates analysis. As expected, the same differential gene expression analysis identified a larger set of differentially expressed genes in the striatum (191 genes). A single factor Deseq2 analysis pointed out 126 genes whose expression was deregulated at PND7 in the striatum of *Thra*$^{AMI/gn}$ mice, compared with age-matched control mice. At PND14, this number raised to 215 genes. Overall, 260 genes were found to be deregulated in the striatum of *Thra*$^{AMI/gn}$ mice at either stage. Eight of these genes (*Cxcl14, Flywch2, Glra3, Ppargc1a, Prox1, Pvalb, Sst, Syt2*) were also deregulated in the cortex. Hierarchical clustering analysis of the striatum data mainly revealed a sharp transition between PND7 and PND14 in the striatum of control mice, which did not take place in *Thra*$^{AMI/gn}$ mice (Figure 5).

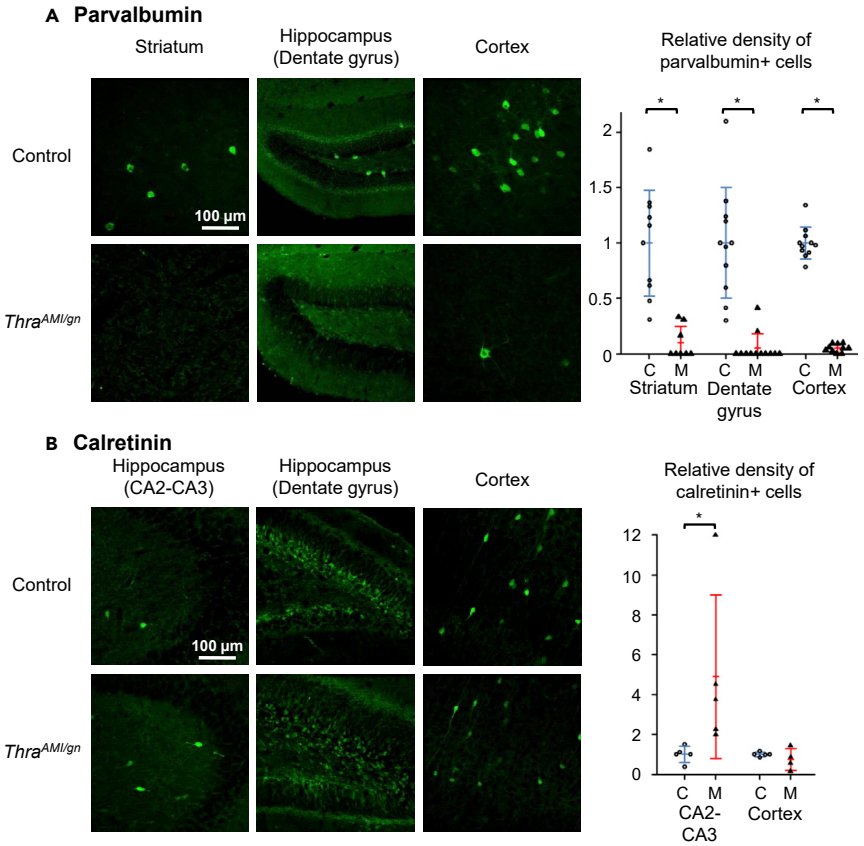

Figure 3. Immunohistochemistry for Parvalbumin and Calretinin

Immunohistochemistry for parvalbumin (A) and calretinin (B) in PND14 *Thra*$^{AMI/gn}$ and control mouse pups in selected brain regions. Right panels: scatterplots illustrating the relative density of immunoreactive cells in control (C, empty circles; blue lines for the mean and standard deviation) and mutant (M, filled triangles; red lines for the mean and standard deviation) mice. Calretinin-immunoreactive neurons could not be quantified in the dentate gyrus, due to the difficulty in delineating individual cells in this area. *$p < 0.05$. See also Figures S4–S7.

These differences in gene expression, as measured by Ampliseq, may have two origins. They can reflect deregulations of the expression of TRα1 target genes in GABAergic neurons, but they can also reflect various indirect consequences of these deregulations, such as a change in the composition of the cell population. In order to pinpoint the TRα1 target genes within the set of differentially expressed genes in striatum, we crossed the above results with a dataset obtained in wild-type mice, comparing different hormonal statuses. We assumed that the expression of TRα1 target genes should be quickly modified by changes in TH levels, whereas indirect consequences should be much slower. In the dataset, 181 genes were found to be deregulated in the striatum of hypothyroid mice, whereas 86 genes responded to a 2-day TH treatment of hypothyroid mice (Dataset S1). RT-qPCR was used to confirm some of these observations (Tables S2–S4). In this dataset, however, the response of GABAergic neurons to TH cannot be distinguished from the response of other cell types present in the striatum, which also express TRα1. The overlap between the two datasets pointed out a set of 38 TH-activated genes whose expression pattern suggested a direct regulation by TRα1 in GABAergic neurons, whereas only 1 gene displayed an expression pattern that suggests a negative regulation by T3-bound TRα1 (Figure 6A).

Identification of Direct TRα1 Target Genes in GABAergic Neurons of the Striatum

To complete the identification of TRα1 target genes in striatal GABAergic neurons, we analyzed chromatin occupancy by TRα1 at a genome-wide scale by ChIPseq. Using *Thra*$^{TAG/gn}$ mice, we precipitated the DNA/protein complexes, which contain the tagged TRα1 from the whole striatum, to address chromatin occupancy in GABAergic neurons only. This experiment revealed the existence of 7,484 chromatin sites

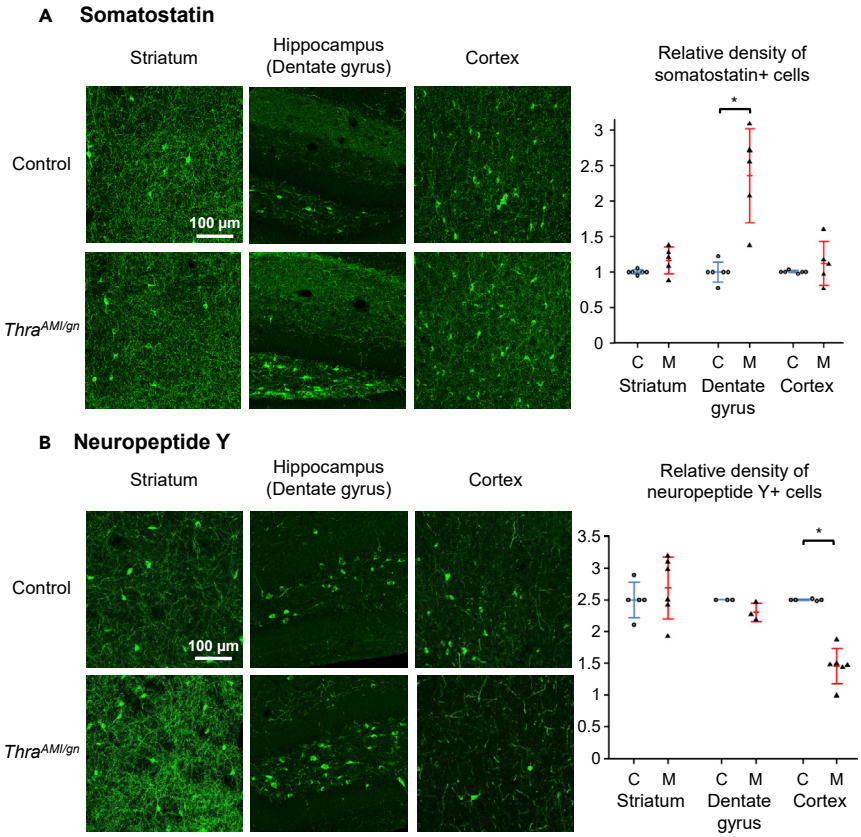

Figure 4. Immunohistochemistry for Somatostatin and Neuropeptide Y

Immunohistochemistry for somatostatin (A) and neuropeptide Y (B) in PND14 *Thra*$^{AMI/gn}$ and control mouse pups in the striatum, hippocampus, and cortex. Right panels: scatterplots illustrating the relative density of immunoreactive cells in control (C, empty circles; blue lines for the mean and standard deviation) and mutant (M, filled triangles; red lines for the mean and standard deviation) mice. *p < 0.05. See also Figures S6 and S7.

occupied by TRα1^{TAG} (thyroid hormone receptor binding sites = TRBSs) in the genome (Figure 6B). In agreement with our previous study (Chatonnet et al., 2013) *de novo* motif discovery (http://meme-suite.org/tools/meme-chip) and enrichment analysis revealed a single consensus sequence for the binding of TRα1/RXR heterodimers. The sequence is the so-called DR4 element (Figure 6C). Assuming that proximity (<30kb) between the TRα1^{TAG} binding site and the transcription start site is sufficient for direct transcriptional regulation by TRα1 would lead to consider a large fraction of genes as putative target genes (3,979/23,931 annotated genes in the mouse genome mm10 version; 16.6%). Among the 38 genes that are sensitive to TRα1^{L400R} expression and hypothyroidism and responsive to TH in hypothyroid mice, genes with a proximal TRBS were overrepresented (35/38: 92%; enrichment of 5.5 compared with the whole set of annotated genes). Interestingly, this enrichment was more striking if we considered only the TRBSs where a DR4 element was identified (3,813/7,484; 51%): DR4 elements were present within 30 kb of 7.5% of annotated genes (1,786/23,931) and of 45% of the putative TRα1 target genes identified in the present study (17/38) (Figure 6D). The same reasoning leads to the conclusion that the transcription of genes that are downregulated after T3 treatment is not regulated by chromatin-bound TRα1 (Figure 6D). Overall, the ChipSeq dataset suggests that a large fraction of the TRBS does not reflect the binding of TRα1/RXR heterodimers to DR4 elements but corresponds to other modes of chromatin association, which do not necessarily promote TH-mediated transactivation. However, as we cannot rule out that other types of response elements are also used, this analysis leaves us with 35 genes, which meet all the criteria for being considered as TRα1 direct target genes. Although some of these genes are known to have a neurodevelopmental function, they do not fall into a specific ontological category (Table S5). This implies that TH promotes GABAergic neuron maturation by simultaneously acting on different cell compartments and cellular pathways.

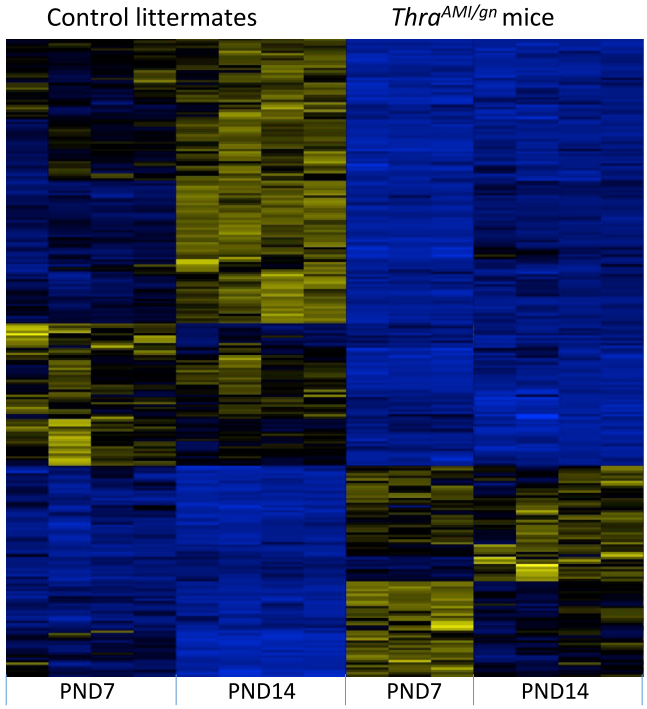

Figure 5. Differentially Expressed Genes in the Striatum

Hierarchical clustering analysis of differentially expressed transcripts in the striatum of *Thra*$^{AMI/gn}$ mice and control littermates at PND7 and PND14. The analysis is restricted to 260 genes for which the fold-change is > 2 or <0.5 (adjusted p value < 0.05) for at least one developmental stage. High expression is in yellow, low expression is in blue, average in black. Note that the changes in gene expression between PND7 and PND14 are more conspicuous in control than in mutant mice, suggesting that a maturation process is blunted by the mutation. See also Figure S8 and Tables S2 and S4.

DISCUSSION

Using two mouse models expressing mutant forms of TRα1 specifically in GABAergic neurons, we present evidence showing that TH, bound to TRα1, is required for the late steps of development of GABAergic neurons. As in the present study we have used GABAergic-specific somatic mutations, we can ascertain that the observed defects are cell-autonomous consequences of impaired TH signaling. We found that the defect in GABAergic differentiation is not restricted to a specific brain area, nor to a specific subtype of GABAergic neurons, as several subtypes of both projecting neurons and interneurons were affected by TRα1 mutations. This suggests that, although GABAergic neurons of different brain areas have different embryonal origins (Leto et al., 2006; Marin and Muller, 2014), they share a common pathway of maturation that depends on TH/TRα1 signaling. Transcriptome analysis revealed a significant overlap between the regulated genes of mutant mice in the cortex, where most GABAergic neurons are interneurons, and in the striatum, which is mainly populated by projecting GABAergic neurons, i.e., medium spiny neurons.

These results extend previous findings, obtained either in hypothyroid rodents or in mice with *Thra* mutations, demonstrating the role of TH in GABAergic neurons in the cerebellum (Fauquier et al., 2011; Manzano et al., 2007), striatum (Diez et al., 2008), cortex (Wallis et al., 2008), hippocampus (Navarro et al., 2015), and hypothalamus (Harder et al., 2018). The major contribution of the present work is to demonstrate that the effect of TH/TRα1 on GABAergic neuron development is cell-autonomous. In many respects, neurodevelopmental damage caused by TRα1^{L400R} and TRα1^{E395fs401X} appears to be similar to, but more dramatic than, that reported for the ubiquitous TRα1^{R384C} mutation (Wallis et al., 2008), which is impaired in its affinity for TH, but possesses a residual capacity to transactivate gene expression (Tinnikov et al., 2002). The effects reported here with *Thra* knock-in mutations are also congruent with, although much stronger than, those previously reported in the brains of *Thra KO* mice (Guadano-Ferraz et al., 2003). This difference is not a surprise and has been previously shown to derive from the permanent transcriptional repression exerted by TRα1^{L400R} and TRα1^{E395fs401X} in presence or absence of TH (Flamant et al.,

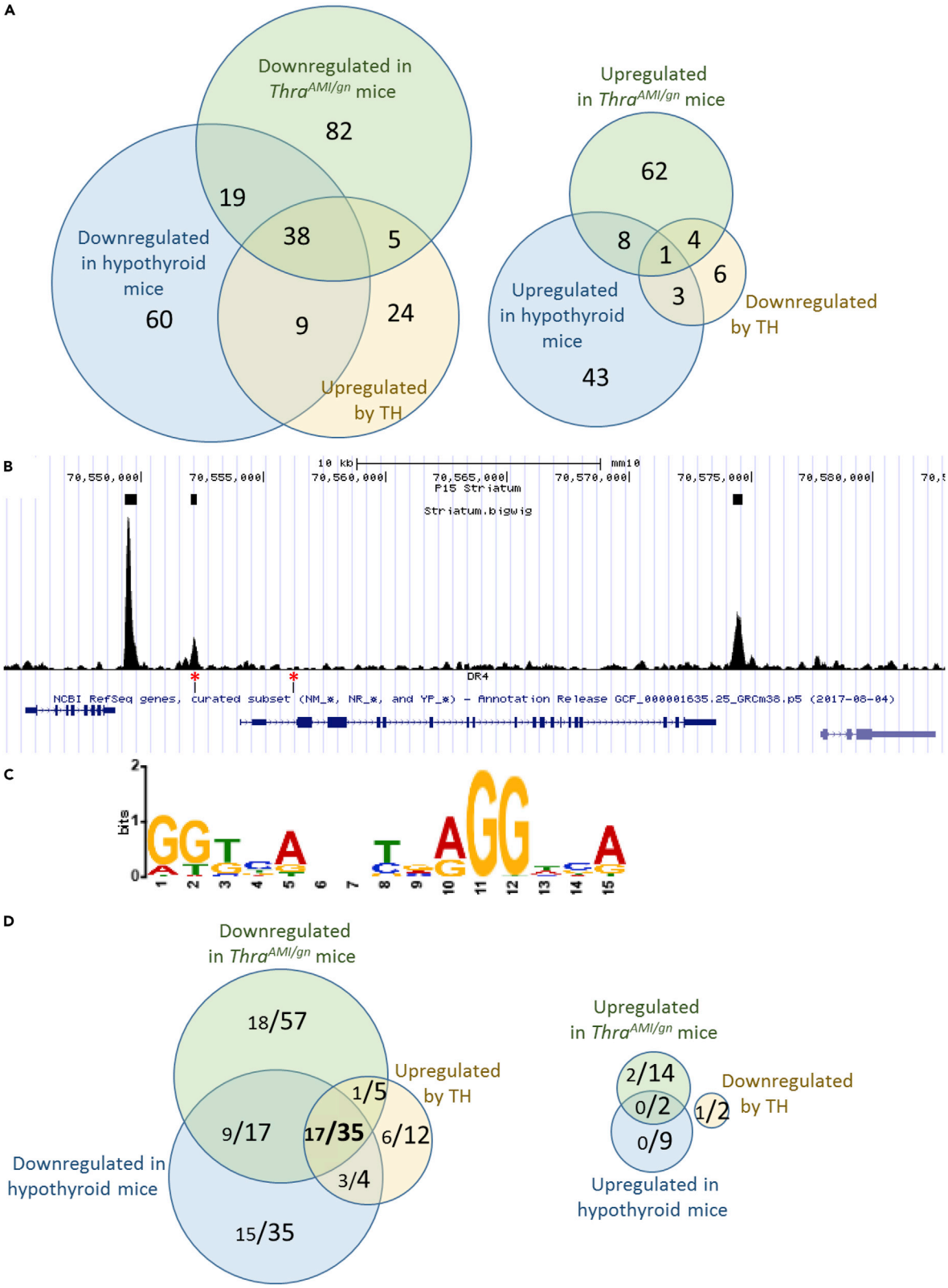
A
Downregulated in Thra^AMI/gn mice
82
19
38
5
Downregulated in hypothyroid mice
60
9
24
Upregulated by TH
Upregulated in Thra^AMI/gn mice
62
8
1
4
6
3
Upregulated in hypothyroid mice
43
Downregulated by TH
B
10 kb
mm10
70,550,000
70,555,000
70,560,000
70,565,000
70,570,000
70,575,000
70,580,000
P15 Striatum
Striatum.bigwig
DR4
NCBI RefSeq genes, curated subset (NM_*, NR_*, and YP_*) - Annotation Release GCF_000001635.25_GRCm38.p5 (2017-08-04)
C
bits
D
Downregulated in Thra^AMI/gn mice
18/57
1/5
Upregulated by TH
9/17
17/35
6/12
3/4
Downregulated in hypothyroid mice
15/35
Upregulated in Thra^AMI/gn mice
2/14
0/2
1/2
Downregulated by TH
0/9
Upregulated in hypothyroid mice

Figure 6. Identifying a Core Set of TRα1 Target Genes in GABAergic Neurons of the Striatum by Combining RNAseq and Chip-Seq Analyses

(A) RNAseq identifies a set of 38 genes, the expression pattern of which is fully consistent with a positive regulation by TRα1, and only 1 gene that has the opposite expression pattern.

(B) Extract of the *Mus musculus* genome browser, around the *Hr* gene, a well-characterized TRα1 target gene. The 3 upper boxes indicate TRBSs identified as significant by the MACS2 algorithm. Note that a DR4-like element (lower track, red asterisks), as defined below, is found in only one of the 3 peaks.

(C) Consensus sequence found in TRBSs identified by *de novo* motif search is close to the DR4 consensus (5′AGGTCANNNNAGGTCA-3′).

(D) Combinations of RNAseq and Chip-Seq data. In the Venn diagrams, each fraction gives the number of genes with a proximal TRBS (<30 kb for transcription start site, large lettering) and, among these genes, those in which a DR4 element was identified (small lettering). A set of 35 genes fulfill the criteria for being considered as genuine TRα1 target genes: they are downregulated in hypothyroid and mutant mice and upregulated after TH treatment of hypothyroid mice. For 17 of these genes, the TRBS contains a recognizable DR4-like element.

See also Data S1 and Tables S2–S5.

2017). The transcriptional repression effect exerted by unliganded TRα is completely lost in *Thra KO* mice, resulting in a much milder phenotype.

The present data indicate that TRα1 plays a major role in the late steps of development of several categories of GABAergic neurons. This is most obvious for PV + interneurons, which almost disappear from several brain areas in $Thra^{AMI/gn}$ mice. However, their progenitors appear to be present, as evidenced by the use of tdTomato as a reporter for cells of the GABAergic lineage. Thus, we can exclude that TRα1 plays a major role in the first steps of GABAergic neuron development, i.e., progenitor proliferation and migration.

In the hippocampus, the density of tdTomato+ and CR + cells was higher in $Thra^{AMI/gn}$ mice than in controls, and the limits of the granular layer were blurred. These results are congruent with previous studies. Indeed, blurring of the borders of the granular layers has been observed in hypothyroid rats (Navarro et al., 2015). An increase in CR + cells has also been reported in the hippocampus of mice expressing $TR\alpha^{R384C}$ (Hadjab-Lallemend et al., 2010). Thus, we can speculate that TH signaling in GABAergic neurons plays a role in the process of lamination in the hippocampus. In particular, the increase in tdTomato + cells in the hippocampus of $Thra^{AMI/gn}$ mice may result from impaired cell apoptosis, possibly affecting CR neurons.

The fate of the progenitors that fail to express PV in $Thra^{AMI/gn}$ mice is unclear. One hypothesis is that they commit to a different GABAergic lineage. This could notably explain the excess of SST + cells in the hippocampus, because PV+ and SST + cortical interneurons share the same precursors (Hu et al., 2017; Mukhopadhyay et al., 2009). However, the results obtained in the cortex do not support such hypothesis, because the density of SST + cells in the cortex did not differ between $Thra^{AMI/gn}$ mice and their control littermates. An alternative hypothesis would be that the effects observed in different categories of GABAergic neurons are secondary to the near disappearance of PV + interneurons. Indeed, many defects caused by hypothyroidism in the brain are indirect, some of them being secondary to a defect in neurotrophin secretion in the microenvironment (Bernal, 2002; Giordano et al., 1992; Neveu and Arenas, 1996; Yu et al., 2015).

Our genome-wide search pinpointed a small set of genes fulfilling the criteria, which lead us to consider them as genuine TRα1 target genes in GABAergic neurons: (1) the mRNA level of these genes is TH responsive, (2) it is decreased in the striatum of $Thra^{AMI/gn}$ mice, and (3) TRα1 occupies a chromatin binding site located at a limited distance of their transcription start site. The last criterion is important, as it helps to differentiate between direct and indirect influences of TRα1 on gene regulation. Thus, we have addressed chromatin occupancy by TRα1 *in vivo*, in the striatum. Importantly, we have used a genetic strategy enabling to selectively identify GABAergic neuron-specific TRα1 binding to DNA within a heterogeneous tissue. The large number of chromatin binding sites that we have identified (7,484 TRBS) contrasts with the small set of 35 genes that we have identified as being directly regulated by TRα1 in GABAergic neurons. As we have used stringent statistical thresholds, we have probably overlooked some genuine TRα1 genes. For example, *Klf9* is a known target gene (Chatonnet et al., 2015), which is not present in our list, due to a below-threshold downregulation in the striatum of hypothyroid mice. However, even with liberal statistical thresholds, the number of presumptive target genes would not exceed 100, a number which is still small compared with the number of genes with a proximal TRBS. Such a contrast has previously been observed in other systems (Ayers et al., 2014; Chatonnet et al., 2013; Grontved et al., 2015; Ramadoss et al., 2014) and suggests that only a small fraction of the TRBSs

are involved in TH-mediated transactivation. Finally, the low level of correspondence between TRBSs and genes that are downregulated after T3 treatment (Figure 6D) suggests that the negative regulation of gene expression exerted by TH is not directly mediated by chromatin-bound TRα1, but perhaps an indirect consequence of the upregulation of transcription inhibitors. Further investigations will be required to better define these active TRBSs and better establish the correspondence between chromatin occupancy and transcriptional regulation by TRα1.

Most of the TRα1 target genes identified in the striatum have already been identified as being sensitive to the local TH level in various brain areas and at different developmental stages (see Table S1 in Chatonnet et al., 2015). This reinforces the hypothesis that they belong to a common genetic program that is regulated by TH, via TRα1, and that promotes the proper maturation of several categories of GABAergic neurons. Although their function in neurons is for a large part unknown, these genes can be grouped according to the putative function of their protein products: *Shh* and *Fgf16* encode secreted proteins, which play major roles in cellular interactions. *Sema7a* and *Nrtn* are involved in axon growth and pathfinding. Others are likely to define the electrophysiological properties of neurons by encoding ion channels *(Kctd17),* transporters of small metabolites *(Slc22a3, Slc26a10),* or modulators of synaptic activity (*Nrgn, Lynx1).*

Overall, the broad influence of TRα1 mutations on GABAergic neuron differentiation and maturation is expected to greatly and permanently impair brain function, notably in the cortex, where a subtle equilibrium between different GABAergic neuron subtypes is necessary for normal development and plasticity (Butt et al., 2017). In the mouse models presented here, epileptic seizures appear to be a main cause of mortality, which sheds light on the cause of the lethality that had been previously observed in mice with different *Thra* mutations (Fraichard et al., 1997; Kaneshige et al., 2001; Tinnikov et al., 2002) as well as in mice suffering from complete TH deprivation (Flamant et al., 2002; Mansouri et al., 1998). Of note, the increase in NPY intensity that we have reported in the striatum and hippocampus of mutant mice may be secondary to the occurrence of epileptic seizures in these mice. Indeed, epileptic seizures are known to increase the expression of NPY in various brain regions, including the hippocampus (Husum et al., 2002; Vezzani and Sperk, 2004). The epileptic phenotype induced in mice by expressing a *Thra* mutation in GABAergic neurons is highly relevant to human pathology, as a history of epilepsy has been reported for several of the rare patients with a *THRA* mutation (Moran and Chatterjee, 2016). Autism spectrum disorders (ASD), whose comorbidity with epilepsy is well documented, have also been reported in these patients (Kalikiri et al., 2017; Yuen et al., 2015). It is likely that these pathological traits are also due to a defect in GABAergic neuron maturation, and our data suggest that these patients might benefit from a treatment with GABA receptor agonists.

Limitations of the Study

The modified *Thra* alleles used in the present study ($Thra^{AMI}$, $Thra^{Slox}$ and $Thra^{TAG}$) result from an extensive remodeling of the *Thra* gene, which eliminates all the *Thra*-encoded proteins except for the mutated receptor. We have shown previously that such elimination of alternate splicing from the *Thra* locus resulted in a moderate overexpression of the mutant allele, compared with the wild-type allele. This overexpression is likely to lead to exaggerated phenotypic manifestations (Markossian et al., 2018). Such exaggerated phenotype has proved efficient in bringing to light key mechanisms by which TH/TRα1 signaling impacts brain development, but the clinical relevance of these mouse models is questionable. Importantly, a similar, albeit milder phenotype has been evidenced in GABAergic neurons of CRISPR/Cas9-generated mice with *Thra* mutations, which are more relevant models of the human RTHα disease (Markossian et al., 2018). Moreover, the epileptic phenotype observed in $Thra^{AMI/gn}$ and $Thra^{Slox/gn}$ mice appears to be congruent with the high occurrence of epilepsy, which has been reported in patients with RTHα (Moran and Chatterjee, 2015; van Gucht et al., 2017). Thus, the mouse models used in the present study appear as relevant for the study of the mechanisms of TH/TRα1 during brain development, even though they do not faithfully mimic the human disease.

A second limitation lies in the use of TRBSs as indicators of direct TRα1 target genes. The conventional strategy, which only takes into account the distance between a TRBS and the nearest transcription start site, has limited value, as nuclear receptors sometimes act at very long distances due to chromosomal looping (Bagamasbad et al., 2008; Buisine et al., 2015, 2018) Further investigations will be required to better define the correspondence between chromatin occupancy by TRα1 and transcriptional regulation.

METHODS

All methods can be found in the accompanying Transparent Methods supplemental file.

DATA AND CODE AVAILABILITY

RNASeq and ChipSeq data are accessible through GEO Series accession number GSE143933 (https://www.ncbi.nlm.nih.gov/geo/query/acc.cgi?acc=GSE143933).

SUPPLEMENTAL INFORMATION

Supplemental Information can be found online at https://doi.org/10.1016/j.isci.2020.100899.

ACKNOWLEDGMENTS

We thank Catherine Etter, Lucas Jacquin, FlorentDelannoy, and Victor Valcárcel, who contributed to histological studies, TiphanyLaurens, who contributed to behavioral analyses, and Karine Gauthier, who performed *in vivo* experiments with propylthiouracil/TH treatments. We thank Nadine Aguilera, Marie Teixeira, and the ANIRA-PBES facility for help in transgenesis and mouse breeding. We also thank Benjamin Gillet, Sandrine Hughes, and the PSI platform of IGFL for deep DNA sequencing. Finally, we thank Emmanuel Quemener from Center Blaise Pascal/ENSL for the development and maintenance of the ENS Galaxy portal with the help of SIDUS (Single Instance Distributing Universal System). This work was supported by grants from the French Agence Nationale de la Recherche (Thyromut2 program; ANR-15-CE14-0011-01) and from the European Union's Horizon 2020 research and innovation program under grant agreement no. 825753 (ERGO).

AUTHOR CONTRIBUTIONS

FF, SR, and RG conceived the study. SM and DA created the genetically modified mouse lines. SR characterized the histological and behavioral phenotype of the mice. RG, MRM, MP, and FF carried out the transcriptome and ChipSeq experiments. FF and SR wrote the manuscript. All authors reviewed and commented on the final manuscript.

DECLARATION OF INTERESTS

The authors declare no competing interest.

Received: June 3, 2019
Revised: December 12, 2019
Accepted: February 5, 2020
Published: March 27, 2020

REFERENCES

Ayers, S., Switnicki, M.P., Angajala, A., Lammel, J., Arumanayagam, A.S., and Webb, P. (2014). Genome-wide binding patterns of thyroid hormone receptor Beta. PLoS One *9*, e81186.

Bagamasbad, P., Howdeshell, K.L., Sachs, L.M., Demeneix, B.A., and Denver, R.J. (2008). A role for basic transcription element-binding protein 1 (BTEB1) in the autoinduction of thyroid hormone receptor beta. J. Biol. Chem. *283*, 2275–2285.

Berbel, P., Marco, P., Cerezo, J.R., and DeFelipe, J. (1996). Distribution of parvalbumin immunoreactivity in the neocortex of hypothyroid adult rats. Neurosci. Lett. *204*, 65–68.

Berbel, P., Navarro, D., and Roman, G.C. (2014). An evo-devo approach to thyroid hormones in cerebral and cerebellar cortical development: etiological implications for autism. Front. Endocrinol. *5*, 146.

Bernal, J. (2002). Action of thyroid hormone in brain. J. Endocrinol. Invest. *25*, 268–288.

Bernal, J., Guadano-Ferraz, A., and Morte, B. (2003). Perspectives in the study of thyroid hormone action on brain development and function. Thyroid *13*, 1005–1012.

Bradley, D.J., Young, W.S., 3rd, and Weinberger, C. (1989). Differential expression of alpha and beta thyroid hormone receptor genes in rat brain and pituitary. Proc. Natl. Acad. Sci. U S A *86*, 7250–7254.

Buisine, N., Ruan, X., Bilesimo, P., Grimaldi, A., Alfama, G., Ariyaratne, P., Mulawadi, F., Chen, J., Sung, W.K., Liu, E.T., et al. (2015). Xenopus tropicalis genome Re-scaffolding and Re-annotation reach the resolution required for in vivo ChIA-PET analysis. PLoS One *10*, e0137526.

Buisine, N., Ruan, X., Ruan, Y., and Sachs, L.M. (2018). Chromatin interaction analysis using paired-end-tag (ChIA-PET) sequencing in tadpole tissues. Cold Spring Harb. Protoc. https://doi.org/10.1101/pdb.prot104620.

Burckstummer, T., Bennett, K.L., Preradovic, A., Schutze, G., Hantschel, O., Superti-Furga, G., and Bauch, A. (2006). An efficient tandem affinity purification procedure for interaction proteomics in mammalian cells. Nat. Methods *3*, 1013–1019.

Butt, S.J., Stacey, J.A., Teramoto, Y., and Vagnoni, C. (2017). A role for GABAergic interneuron diversity in circuit development and plasticity of the neonatal cerebral cortex. Curr. Opin. Neurobiol. *43*, 149–155.

Chatonnet, F., Flamant, F., and Morte, B. (2015). A temporary compendium of thyroid hormone target genes in brain. Biochim. Biophys. Acta *1849*, 122–129.

Chatonnet, F., Guyot, R., Benoit, G., and Flamant, F. (2013). Genome-wide analysis of thyroid hormone receptors shared and specific functions in neural cells. Proc. Natl. Acad. Sci. U S A *110*, E766–E775.

DeFelipe, J., Lopez-Cruz, P.L., Benavides-Piccione, R., Bielza, C., Larranaga, P., Anderson, S., Burkhalter, A., Cauli, B., Fairen, A., Feldmeyer, D., et al. (2013). New insights into the classification and nomenclature of cortical GABAergic interneurons. Nat. Rev. Neurosci. *14*, 202–216.

Diez, D., Grijota-Martinez, C., Agretti, P., De Marco, G., Tonacchera, M., Pinchera, A., de Escobar, G.M., Bernal, J., and Morte, B. (2008). Thyroid hormone action in the adult brain: gene expression profiling of the effects of single and multiple doses of triiodo-L-thyronine in the rat striatum. Endocrinology *149*, 3989–4000.

Fauquier, T., Chatonnet, F., Picou, F., Richard, S., Fossat, N., Aguilera, N., Lamonerie, T., and Flamant, F. (2014). Purkinje cells and Bergmann glia are primary targets of the TRalpha1 thyroid hormone receptor during mouse cerebellum postnatal development. Development *141*, 166–175.

Fauquier, T., Romero, E., Picou, F., Chatonnet, F., Nguyen, X.N., Quignodon, L., and Flamant, F. (2011). Severe impairment of cerebellum development in mice expressing a dominant-negative mutation inactivating thyroid hormone receptor alpha1 isoform. Dev. Biol. *356*, 350–358.

Fetene, D.M., Betts, K.S., and Alati, R. (2017). Mechanisms IN endocrinology: maternal thyroid dysfunction during pregnancy and behavioural and psychiatric disorders of children: a systematic review. Eur. J. Endocrinol. *177*, R261–R273.

Filice, F., Vorckel, K.J., Sungur, A.O., Wohr, M., and Schwaller, B. (2016). Reduction in parvalbumin expression not loss of the parvalbumin-expressing GABA interneuron subpopulation in genetic parvalbumin and shank mouse models of autism. Mol. Brain *9*, 10.

Flamant, F., Gauthier, K., and Richard, S. (2017). Genetic investigation of thyroid hormone receptor function in the developing and adult brain. Curr. Top. Dev. Biol. *125*, 303–335.

Flamant, F., Poguet, A.L., Plateroti, M., Chassande, O., Gauthier, K., Streichenberger, N., Mansouri, A., and Samarut, J. (2002). Congenital hypothyroid Pax8(-/-) mutant mice can be rescued by inactivating the TRalpha gene. Mol. Endocrinol. *16*, 24–32.

Fraichard, A., Chassande, O., Plateroti, M., Roux, J.P., Trouillas, J., Dehay, C., Legrand, C., Gauthier, K., Kedinger, M., Malaval, L., et al. (1997). The T3R alpha gene encoding a thyroid hormone receptor is essential for post-natal development and thyroid hormone production. EMBO J. *16*, 4412–4420.

Gil-Ibanez, P., Bernal, J., and Morte, B. (2014). Thyroid hormone regulation of gene expression in primary cerebrocortical cells: role of thyroid hormone receptor subtypes and interactions with retinoic acid and glucocorticoids. PLoS One *9*, e91692.

Giordano, T., Pan, J.B., Casuto, D., Watanabe, S., and Arneric, S.P. (1992). Thyroid hormone regulation of NGF, NT-3 and BDNF RNA in the adult rat brain. Brain Res. Mol. Brain Res. *16*, 239–245.

Grontved, L., Waterfall, J.J., Kim, D.W., Baek, S., Sung, M.H., Zhao, L., Park, J.W., Nielsen, R., Walker, R.L., Zhu, Y.J., et al. (2015). Transcriptional activation by the thyroid hormone receptor through ligand-dependent receptor recruitment and chromatin remodelling. Nat. Commun. *6*, 7048.

Guadano-Ferraz, A., Benavides-Piccione, R., Venero, C., Lancha, C., Vennstrom, B., Sandi, C., DeFelipe, J., and Bernal, J. (2003). Lack of thyroid hormone receptor alpha1 is associated with selective alterations in behavior and hippocampal circuits. Mol. Psychiatry *8*, 30–38.

Hadjab-Lallemend, S., Wallis, K., van Hogerlinden, M., Dudazy, S., Nordstrom, K., Vennstrom, B., and Fisahn, A. (2010). A mutant thyroid hormone receptor alpha1 alters hippocampal circuitry and reduces seizure susceptibility in mice. Neuropharmacology *58*, 1130–1139.

Harder, L., Dudazy-Gralla, S., Muller-Fielitz, H., Hjerling Leffler, J., Vennstrom, B., Heuer, H., and Mittag, J. (2018). Maternal thyroid hormone is required for parvalbumin neurone development in the anterior hypothalamic area. J. Neuroendocrinol. *30*, e12573.

Hu, J.S., Vogt, D., Sandberg, M., and Rubenstein, J.L. (2017). Cortical interneuron development: a tale of time and space. Development *144*, 3867–3878.

Husum, H., Gruber, S.H., Bolwig, T.G., and Mathe, A.A. (2002). Extracellular levels of NPY in the dorsal hippocampus of freely moving rats are markedly elevated following a single electroconvulsive stimulation, irrespective of anticonvulsive Y1 receptor blockade. Neuropeptides *36*, 363–369.

Kalikiri, M.K., Mamidala, M.P., Rao, A.N., and Rajesh, V. (2017). Analysis and functional characterization of sequence variations in ligand binding domain of thyroid hormone receptors in autism spectrum disorder (ASD) patients. Autism Res. *10*, 1919–1928.

Kaneshige, M., Suzuki, H., Kaneshige, K., Cheng, J., Wimbrow, H., Barlow, C., Willingham, M.C., and Cheng, S. (2001). A targeted dominant negative mutation of the thyroid hormone alpha 1 receptor causes increased mortality, infertility, and dwarfism in mice. Proc. Natl. Acad. Sci. U S A *98*, 15095–15100.

Kepecs, A., and Fishell, G. (2014). Interneuron cell types are fit to function. Nature *505*, 318–326.

Leto, K., Carletti, B., Williams, I.M., Magrassi, L., and Rossi, F. (2006). Different types of cerebellar GABAergic interneurons originate from a common pool of multipotent progenitor cells. J. Neurosci. *26*, 11682–11694.

Mansouri, A., Chowdhury, K., and Gruss, P. (1998). Follicular cells of the thyroid gland require Pax8 gene function. Nat. Genet. *19*, 87–90.

Manzano, J., Cuadrado, M., Morte, B., and Bernal, J. (2007). Influence of thyroid hormone and thyroid hormone receptors in the generation of cerebellar gamma-aminobutyric acid-ergic interneurons from precursor cells. Endocrinology *148*, 5746–5751.

Marin, O., and Muller, U. (2014). Lineage origins of GABAergic versus glutamatergic neurons in the neocortex. Curr. Opin. Neurobiol. *26*, 132–141.

Markossian, S., Guyot, R., Richard, S., Teixeira, M., Aguilera, N., Bouchet, M., Plateroti, M., Guan, W., Gauthier, K., Aubert, D., et al. (2018). CRISPR/Cas9 editing of the mouse Thra gene produces models with variable resistance to thyroid hormone. Thyroid *28*, 139–150.

Moran, C., and Chatterjee, K. (2015). Resistance to thyroid hormone due to defective thyroid receptor alpha. Best Pract. Res. Clin. Endocrinol. Metab. *29*, 647–657.

Moran, C., and Chatterjee, K. (2016). Resistance to thyroid hormone alpha-emerging definition of a disorder of thyroid hormone action. J. Clin. Endocrinol. Metab. *101*, 2636–2639.

Mukhopadhyay, A., McGuire, T., Peng, C.Y., and Kessler, J.A. (2009). Differential effects of BMP signaling on parvalbumin and somatostatin interneuron differentiation. Development *136*, 2633–2642.

Navarro, D., Alvarado, M., Navarrete, F., Giner, M., Obregon, M.J., Manzanares, J., and Berbel, P. (2015). Gestational and early postnatal hypothyroidism alters VGluT1 and VGAT bouton distribution in the neocortex and hippocampus, and behavior in rats. Front. Neuroanat. *9*, 9.

Neveu, I., and Arenas, E. (1996). Neurotrophins promote the survival and development of neurons in the cerebellum of hypothyroid rats in vivo. J.Cell Biol. *133*, 631–646.

Picou, F., Fauquier, T., Chatonnet, F., and Flamant, F. (2012). A bimodal influence of thyroid hormone on cerebellum oligodendrocyte differentiation. Mol. Endocrinol. *26*, 608–618.

Picou, F., Fauquier, T., Chatonnet, F., Richard, S., and Flamant, F. (2014). Deciphering direct and indirect influence of thyroid hormone with mouse genetics. Mol. Endocrinol. *28*, 429–441.

Quignodon, L., Vincent, S., Winter, H., Samarut, J., and Flamant, F. (2007). A point mutation in the activation function 2 domain of thyroid hormone receptor alpha1 expressed after CRE-mediated recombination partially recapitulates hypothyroidism. Mol. Endocrinol. *21*, 2350–2360.

Ramadoss, P., Abraham, B.J., Tsai, L., Zhou, Y., Costa-e-Sousa, R.H., Ye, F., Bilban, M., Zhao, K., and Hollenberg, A.N. (2014). Novel mechanism of positive versus negative regulation by thyroid hormone receptor beta1 (TRbeta1) identified by genome-wide profiling of binding sites in mouse liver. J. Biol. Chem. *289*, 1313–1328.

Rovet, J.F. (2014). The role of thyroid hormones for brain development and cognitive function. Endocr. Dev. *26*, 26–43.

Taniguchi, H., He, M., Wu, P., Kim, S., Paik, R., Sugino, K., Kvitsiani, D., Fu, Y., Lu, J., Lin, Y., et al. (2011). A resource of Cre driver lines for genetic targeting of GABAergic neurons in cerebral cortex. Neuron *71*, 995–1013.

Tasic, B., Menon, V., Nguyen, T.N., Kim, T.K., Jarsky, T., Yao, Z., Levi, B., Gray, L.T., Sorensen, S.A., Dolbeare, T., et al. (2016). Adult mouse cortical cell taxonomy revealed by single cell transcriptomics. Nat. Neurosci. *19*, 335–346.

Tinnikov, A., Nordstrom, K., Thoren, P., Kindblom, J.M., Malin, S., Rozell, B., Adams, M., Rajanayagam, O., Pettersson, S., Ohlsson, C., et al. (2002). Retardation of post-natal development caused by a negatively acting thyroid hormone receptor alpha1. EMBO J. *21*, 5079–5087.

van Gucht, A.L.M., Moran, C., Meima, M.E., Visser, W.E., Chatterjee, K., Visser, T.J., and Peeters, R.P. (2017). Resistance to thyroid hormone due to heterozygous mutations in thyroid hormone receptor alpha. Curr. Top. Dev. Biol. *125*, 337–355.

van Mullem, A., van Heerebeek, R., Chrysis, D., Visser, E., Medici, M., Andrikoula, M., Tsatsoulis, A., Peeters, R., and Visser, T.J. (2012). Clinical phenotype and mutant TRα1. N. Engl. J. Med. *366*, 1451–1453.

van Mullem, A.A., Visser, T.J., and Peeters, R.P. (2014). Clinical consequences of mutations in thyroid hormone receptor-alpha1. Eur. Thyroid J. *3*, 17–24.

Vezzani, A., and Sperk, G. (2004). Overexpression of NPY and Y2 receptors in epileptic brain tissue: an endogenous neuroprotective mechanism in temporal lobe epilepsy? Neuropeptides *38*, 245–252.

Wallis, K., Sjogren, M., van Hogerlinden, M., Silberberg, G., Fisahn, A., Nordstrom, K., Larsson, L., Westerblad, H., Morreale de Escobar, G., Shupliakov, O., et al. (2008). Locomotor deficiencies and aberrant development of subtype-specific GABAergic interneurons caused by an unliganded thyroid hormone receptor alpha1. J. Neurosci. *28*, 1904–1915.

Yu, L., Iwasaki, T., Xu, M., Lesmana, R., Xiong, Y., Shimokawa, N., Chin, W.W., and Koibuchi, N. (2015). Aberrant cerebellar development of transgenic mice expressing dominant-negative thyroid hormone receptor in cerebellar Purkinje cells. Endocrinology *156*, 1565–1576.

Yuen, R.K., Thiruvahindrapuram, B., Merico, D., Walker, S., Tammimies, K., Hoang, N., Chrysler, C., Nalpathamkalam, T., Pellecchia, G., Liu, Y., et al. (2015). Whole-genome sequencing of quartet families with autism spectrum disorder. Nat. Med. *21*, 185–191.

iScience, Volume *23*

Supplemental Information

A Pivotal Genetic Program Controlled by Thyroid Hormone during the Maturation of GABAergic Neurons

Sabine Richard, Romain Guyot, Martin Rey-Millet, Margaux Prieux, Suzy Markossian, Denise Aubert, and Frédéric Flamant

Supplemental Information

This section includes:

Figures S1 to S8

Tables S1 to S5

Transparent methods

References for supplemental information

A.

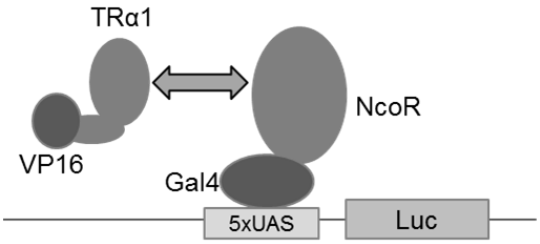

B.

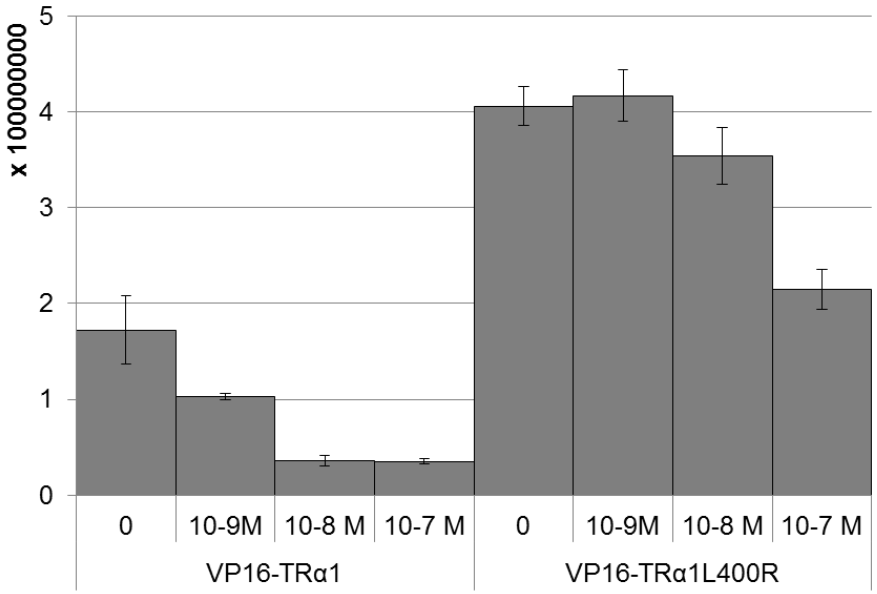

Figure S1. Related to Fig. 1. TRα1^{L400R} ligand binding domain interacts with the NcoR transcription repressor even in the presence of T3. **A.** HEK293 cells, which do not express TRα1, were transfected with 3 plasmids: 1) a construct to drive the expression of a Gal4NcoR fusion protein. 2) A UASLuc construct with binding sites for the Gal4 DNA binding domain. 3) an expression vector to drive the expression of either the VP16-TRα1 or VP16-TRα1^{L400R} fusion. In absence of T3, the interaction between the TRα1 ligand binding domain and NcoR tethers the VP16 activation domain to the UASLuc promoter, resulting in luciferase expression. **B.** T3 addition destabilizes the interaction between TRα1 and NCoR, resulting in decreased luciferase activity. As it is unable to recruit transcription coactivators upon ligand binding, TRα1^{L400R} interacts with NcoR even in the presence of T3.

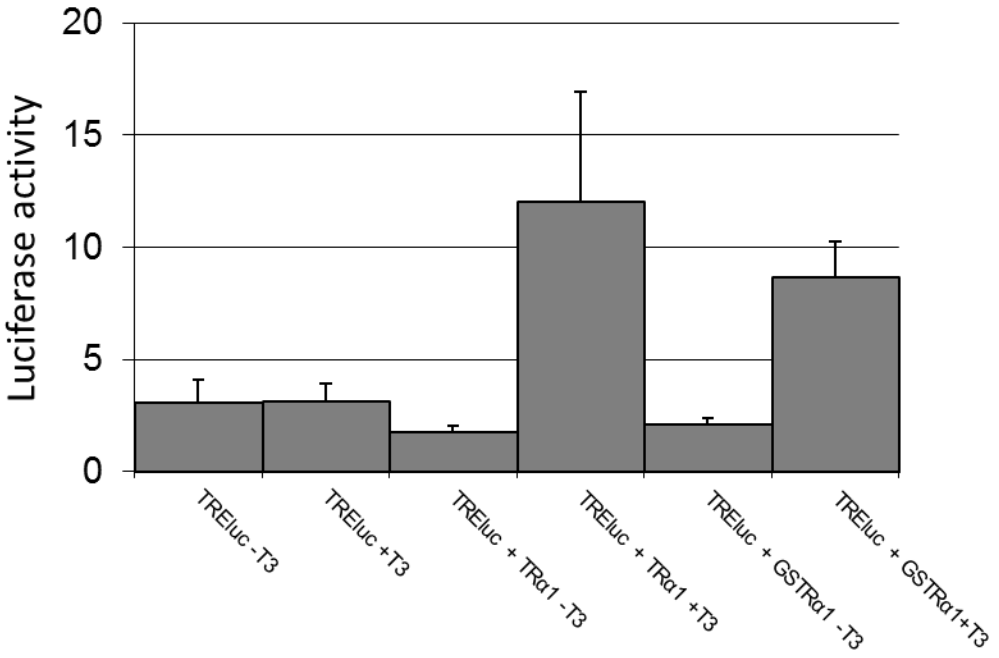

Figure S2. Related to Fig. 1. A N-terminal GS tag does not impair the transactivation capacity of TRα1. HEK293 cells, which do not express TRα1, were transfected with a DR4-driven reporter plasmid construct with the luciferase coding sequence (TREluc) and a SV40-derived vector (pSG5) to drive either TRα1 or GS-TRα1 expression. Cells were then incubated in either control medium (-T3), or T3-supplemented medium (+T3, 10^{-7}M). Luciferase activity was measured 48 hours after transfection. Each transfection was carried out in triplicate.

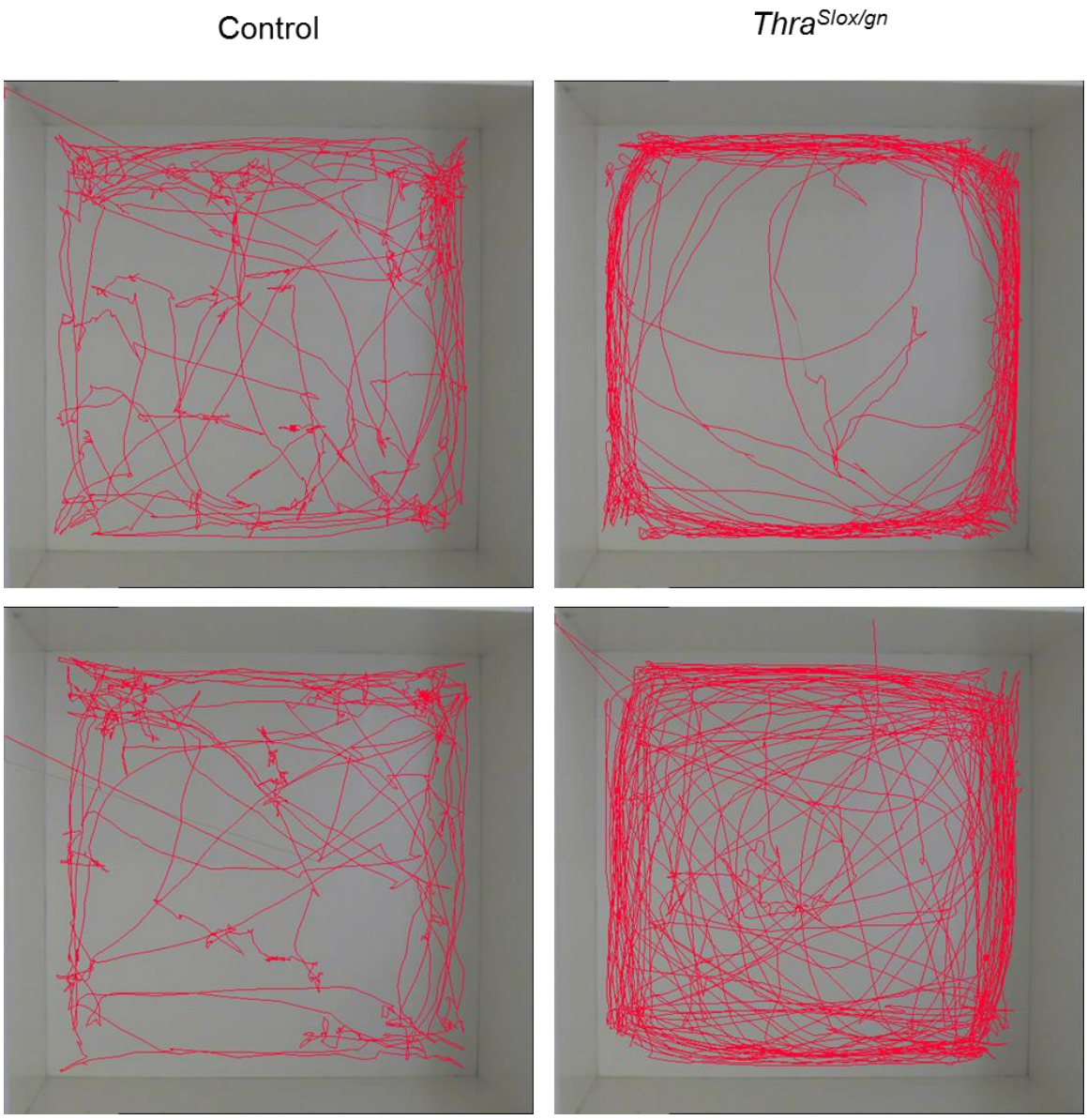

Figure S3. Related to Fig. 1. Representative tracks of adult control (left) and *Thra*$^{Slox/gn}$ (right) mice in a 5-min open-field test.

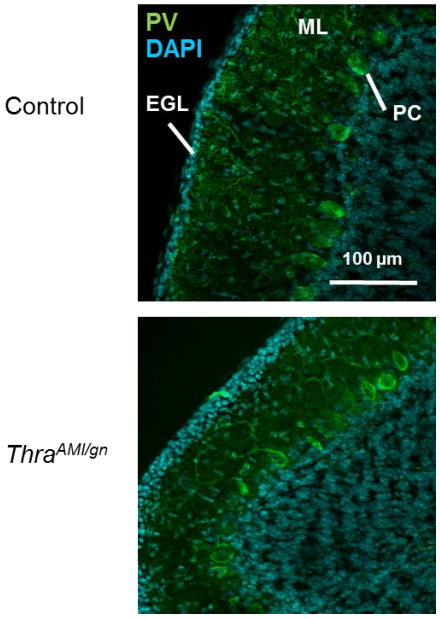

Figure S4. Related to Fig. 3. The cerebellum of PND14 *Thra*$^{AMI/gn}$ exhibits typical hallmarks of hypothyroidism. Fluorescence microscopy images of the cerebellum of PND14 *Thra*$^{AMI/gn}$ and control mouse pups. Green fluorescence labels parvalbumin. Blue fluorescence labels cell nuclei (DAPI labelling). The reduced thickness of the molecular layer (ML) in *Thra*$^{AMI/gn}$ mice, compared to control mice, is related to a reduced arborization of Pukinje cell (PC) dendrites. By contrast, the external granular layer (EGL) is thicker in *Thra*$^{AMI/gn}$ mice than in control mice, which reflects a delay in the migration of granule cells towards the internal granular layer of the cerebellum.

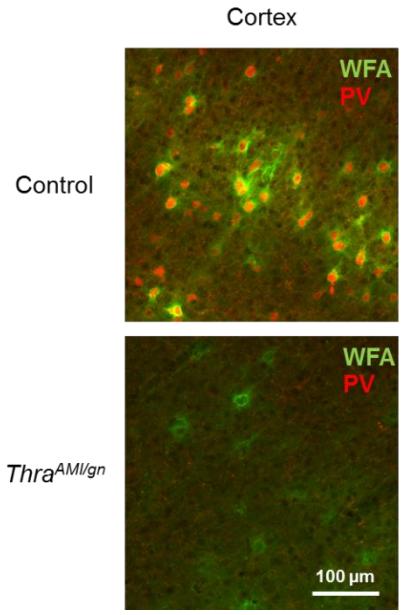

Figure S5. Related to Fig. 3. Perineuronal net formation is greatly impaired in *Thra*$^{AMI/gn}$ mice at PND14. Fluorescence microscopy images of the cortex of PND14 *Thra*$^{AMI/gn}$ and control mouse pups. Green fluorescence labels *Wisteria floribunda* lectin (WFA). Red fluorescence labels parvalbumin (PV). Note that in *Thra*$^{AMI/gn}$ mice, perineuronal nets are formed around cell bodies that are exempt of PV labelling.

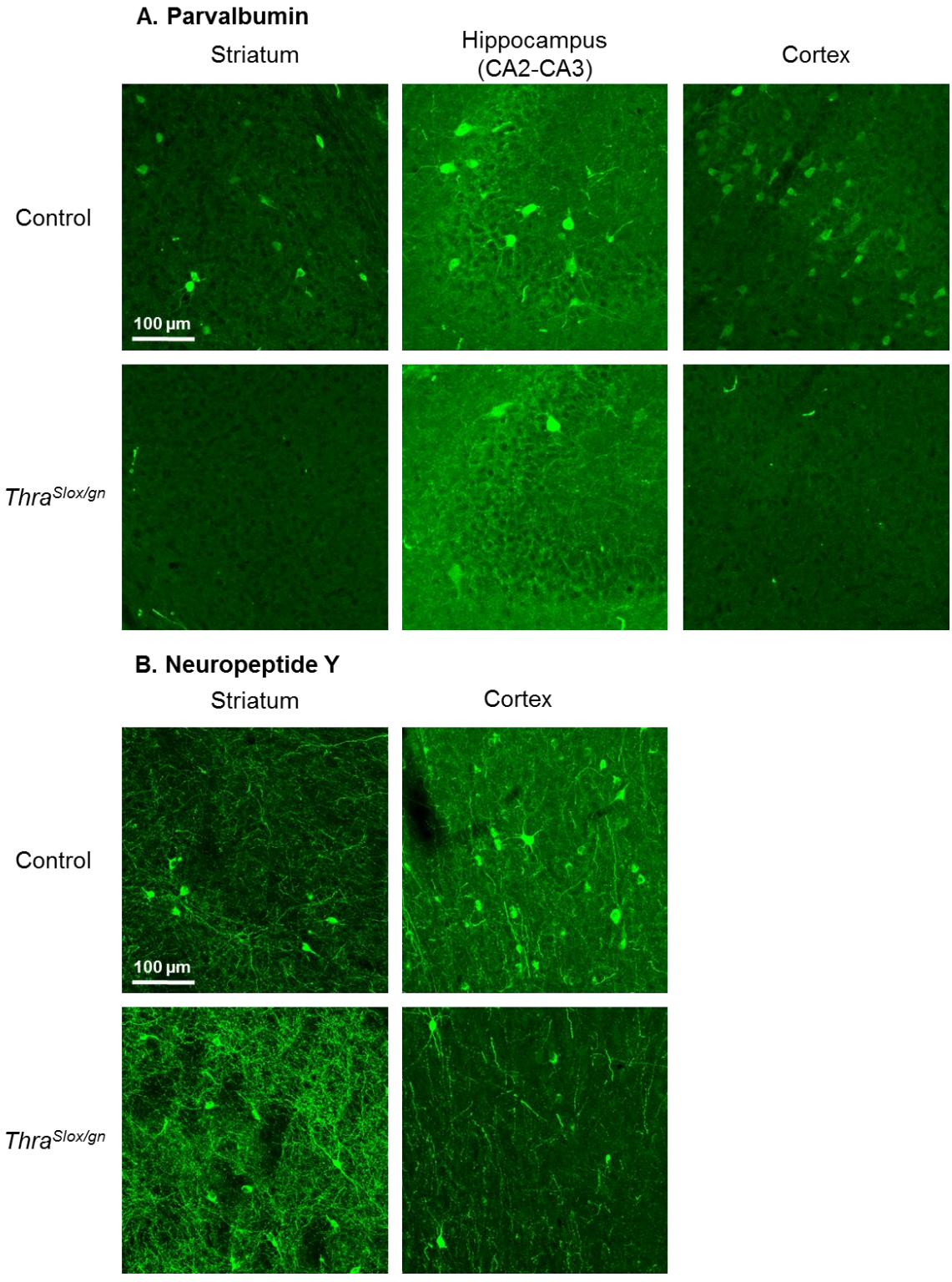

Figure S6. Related to Figs 3 and 4. Immunohistochemistry for parvalbumin (A) and neuropeptide Y (B) in *Thra*$^{Slox/gn}$ and control mouse pups at PND14 in selected brain regions.

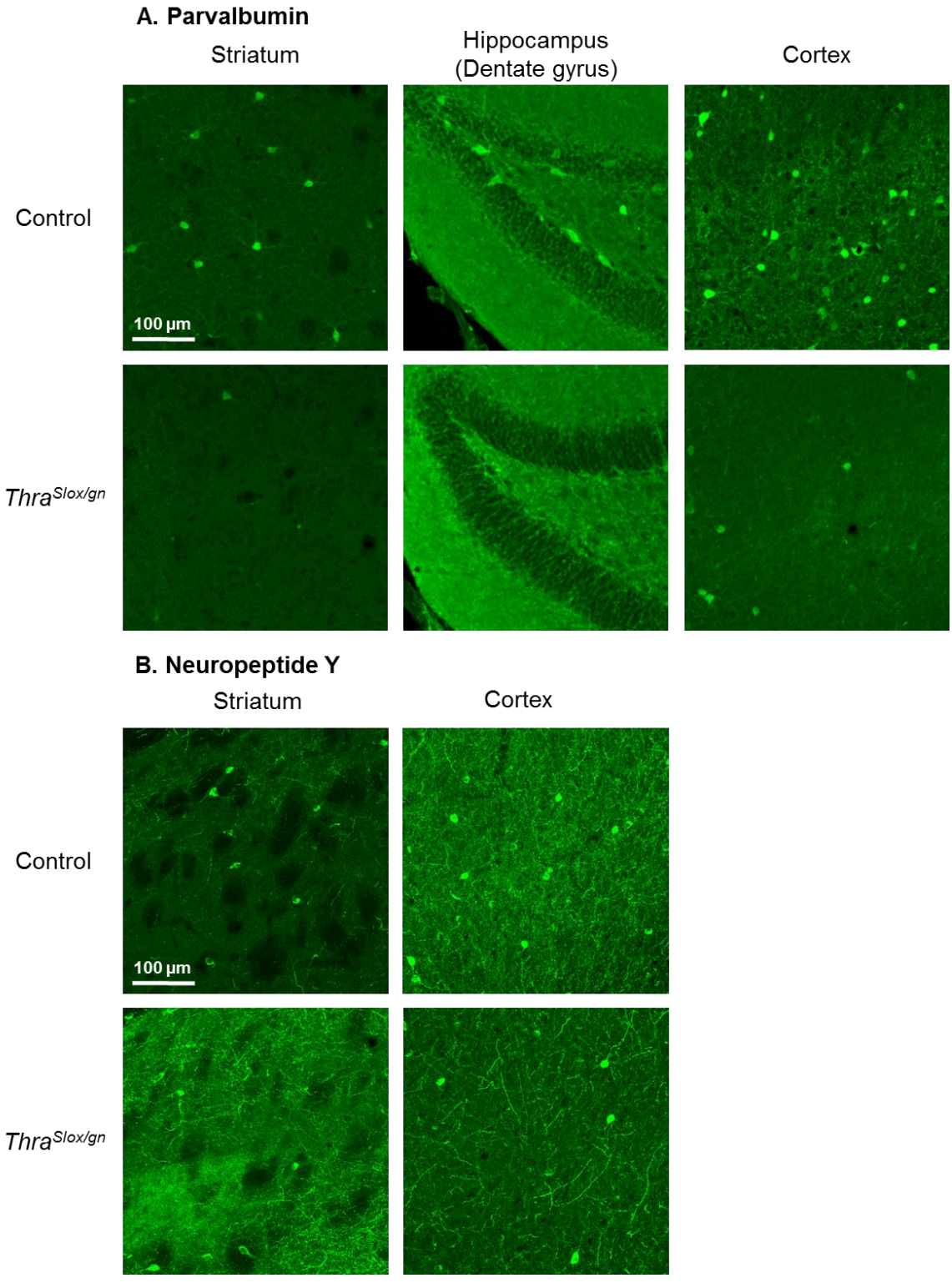

Figure S7. Related to Figs 3 and 4. Immunohistochemistry for parvalbumin (A) and neuropeptide Y (B) in adult *Thra*$^{Slox/gn}$ and control mice in selected brain regions.

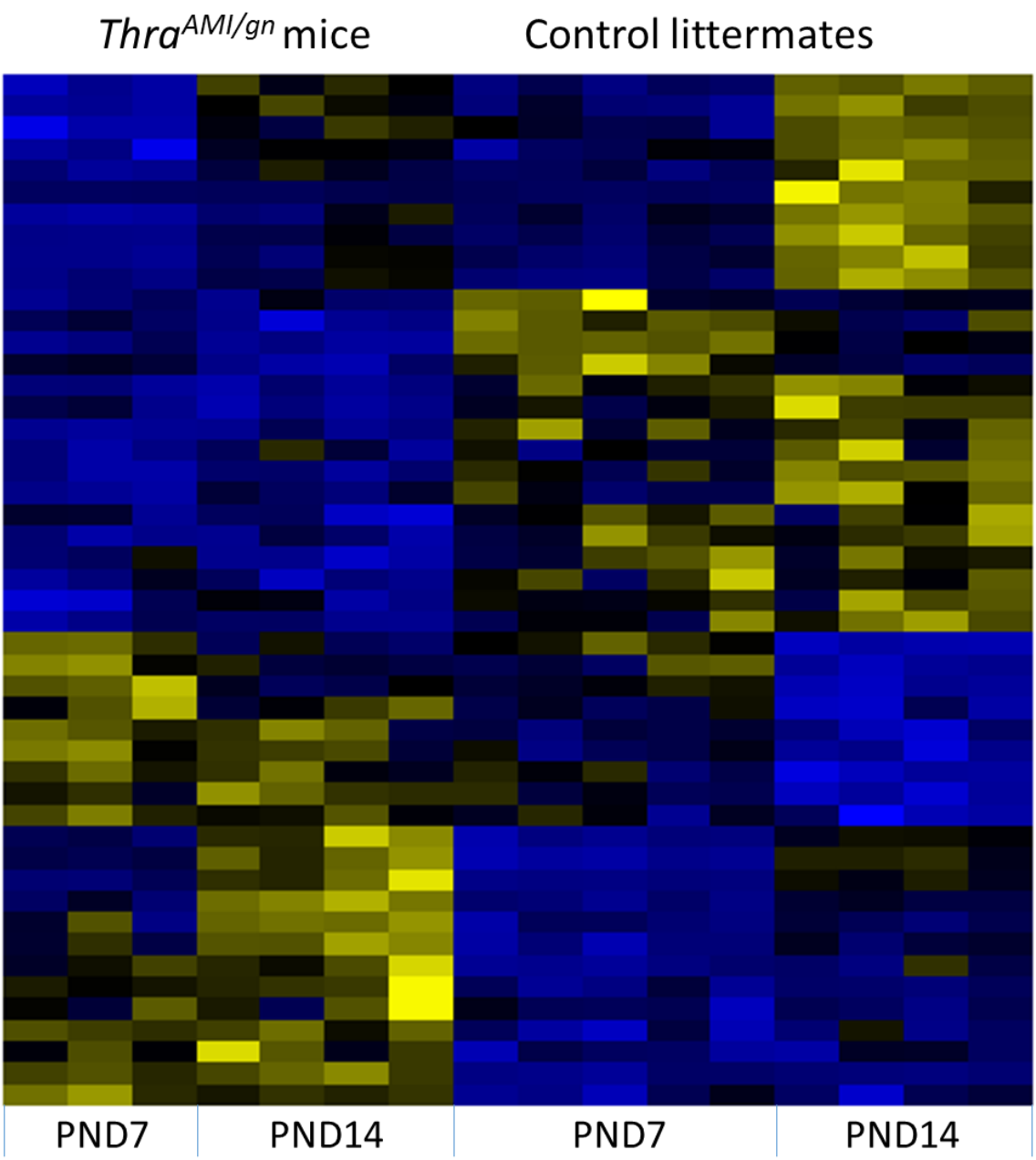

Figure S8. Related to Fig. 5. Hierarchical clustering analysis of differentially expressed transcripts in the cortex of *Thra*$^{AMI/gn}$ mice and control littermates at PND7 and PND14. High expression is in yellow, low expression is in blue, average in black.

Table S1. Related to table 1. Relative abundance of several GABAergic neuron subtypes in. *Thra*$^{Slox/gn}$, compared to control, mouse brains at PND14 and in adults, as evidenced by immunohistochemistry.

			Cortex		Hippocampus (DG)		Hippocampus (CA)		Striatum	
			Control	*Thra* $^{Slox/gn}$	Control	*Thra* $^{Slox/gn}$	Control	*Thra* $^{Slox/gn}$	Control	*Thra* $^{Slox/gn}$
PND14	Parvalbumin neuronal density	Mean	1.00	0.01[a]	nd	nd	1.00	0.56	1.00	0.10[a]
		SD	0.11	0.16	nd	nd	0.17	0.41	0.34	0.27
		n	9	7	nd	nd	8	5	9	7
	Neuropeptide Y neuronal density	Mean	1.00	0.66[a]	nd	nd	nd	nd	1.00	1.31
		SD	0.25	0.26	nd	nd	nd	nd	0.17	0.25
		n	6	6	nd	nd	nd	nd	6	6
	Neuropeptide Y fluorescence intensity	Mean	nd	nd	nd	nd	nd	nd	1.00	1.55[a]
		SD	nd	nd	nd	nd	nd	nd	0.14	0.15
		n	nd	nd	nd	nd	nd	nd	6	6
	Calretinin neuronal density	Mean	1.00	1.23	nd	nd	1.00	2.30[a]	nd	nd
		SD	0.20	0.77	nd	nd	0.17	0.40	nd	nd
		n	7	7	nd	nd	6	3	nd	nd
Adult	Parvalbumin neuronal density	Mean	1.00	0.31[a]	1.00	0.13[a]	1.00	0.50[a]	1.00	0.39[a]
		SD	0.00	0.11	0.00	0.15	0.00	0.29	0.00	0.18
		n	4	4	4	4	4	4	4	4
	Neuropeptide Y neuronal density	Mean	1.00	0.51[a]	nd	nd	nd	nd	1.00	1.22
		SD	0.00	0.12	nd	nd	nd	nd	0.00	0.31
		n	4	4	nd	nd	nd	nd	4	4
	Neuropeptide Y fluorescence intensity	Mean	nd	nd	nd	nd	nd	nd	1.00	1.30[a]
		SD	nd	nd	nd	nd	nd	nd	0.00	0.10
		n	nd	nd	nd	nd	nd	nd	5	5

[a] significantly different from control ($p < 0,05$)

Table S2. Related to Fig. 5. Q-RT-PCR confirmation of the effect of TRα1^{L400R} expression on gene expression in the striatum of *Thra*$^{AMI/gn}$ mice. Data (mean ± standard deviation) are expressed as a fraction of the corresponding gene expression level in control mice. $p < 0.05$ compared to control mice.

Gene	Fold-change PND7	Fold-change PND14
Hr	0.70±0.15	0.70±0.05
Klf9	0.70±0.11	0.28±0.13
Lynx1	0.22±0.05	0.32±0.08
Shh	0.19±0.02	0.21±0.03

n=6

Table S3. Related to Fig.6 and Dataset S1. Q-RT-PCR confirmation of the effect of hypothyroidism and TH stimulation on gene expression in the striatum of PND21 mouse pups. Data (mean ± standard deviation) are expressed as a fraction of the gene expression level in euthyroid mice. For each gene, $p < 0.05$ was found when comparing hypothyroid *vs* euthyroid mice, as well as when comparing hypothyroid+TH *vs* hypothyroid mice.

Gene	Euthyroid	Hypothyroid	Hypothyroid+TH
Ace	1.00±0.06	0.19±0.01	2.06±0.32
Cd72	1.00±0.04	0.05±0.01	0.82±0.13
Col6a1	1.00±0.19	3.21±0.44	2.66±0.17
Dab2ip	1.00±0.05	0.63±0.04	0.95±0.06
Fgf16	1.00±0.06	0.17±0.02	1.58±0.20
Me2	1.00±0.14	0.23±0.02	0.54±0.04
Pvalb	1.00±0.04	0.23±0.07	0.42±0.16
Sema7a	1.00±0.03	0.27±0.02	0.84±0.03
Shh	1.00±0.09	0.32±0.04	1.32±0.14
Slc22a3	1.00±0.10	0.29±0.03	0.79±0.09
Strn	1.00±0.05	0.64±0.02	0.97±0.08

n=8

Table S4. Related to Figs 5 and 6 and to Tables S2 and S3. Q-RT-PCR primers used for gene expression confirmation experiments.

Gene	F primer	R primer
Ace	ACATCAACCTGGATGGCCCC	GTCCATCCCTGCTTTATCATGGC
Cd72	TTCCCCGCTGTCCTACAGTC	TCCTGGAACTGCCGAGACAC
Col6a1	GCCAGCGTGGATGCGGTCAA	GCATCTTCCAGACCCCCGCA
Dab2ip	TCACAGCAGCATCCTGGGTC	CCGGCTGTTGTCCTTGTTGG
Fgf16	ACCGGCTTCCACCTTGAGAT	GCCCCACAGCCAAGCTGATA
HPRT	CAGCGTCGTGATTAGCGATG	CGAGCAAGTCTTTCAGTCCTGTCC
Hr	GCCTTGCTTCCTATGATTGTCTCC	AGAGGTCCAAGGAGCATCAAGG
Klf9	CACGCCTCCGAAAAGAGGCACAA	CTTTTCCCCAGTGTGGGTCCGGTA
Lynx1	TCTGGAGTGCCACGTGTGTG	TGGGGTGAAGTAAGTTCGTGTGG
Me2	CTTCACCCCAGGCCAAGGAA	CTGAGTCGTCAGCGCCTTTG
Pvalb	CTCTGCCCGCTCAAACAGTTG	AGGCCCACCATCTGGAAGAAC
Sema7a	CTTCTGCTGGTGTTCTGGGTGG	GGAAAAGCACGGTGTGTGGC
Shh	GGCCAGCGGCAGATATGAAG	TTTGCACCTCTGAGTCATCAGC
Slc22a3	CGGCTGGCAGCTATATGGTTAG	CTGTGAACTGCCAAGCTTTTCTACG
Strn	TAGAAGCGCAGGCGATGGAAC	TATTGGGCCTCTTCACCCCC

F : Forward orientation R : Reverse. All PCR products are less than 150 bp long.

Table S5 (continued on next page). Related to Figure 6. List of 35 TRα1 direct target genes in mouse striatal GABAergic neurons at PND14, as identified in the present study, using a combination of RNASeq and ChipSeq analyses.

	FC *Thra*$^{AMI/gn}$	FC hypoth.	FC TH response	KO mouse phenotype	Full name
Abcc12	0.44	0.49	2.08	ND	ATP-binding cassette, sub-family C (CFTR/MRP), member 12
Ace	0.15	0.21	8.53	Lethal	angiotensin I converting enzyme (peptidyl-dipeptidase A) 1
Acvr1c	0.19	0.44	2.46	Normal	activin A receptor, type IC
Arg2	0.18	0.49	2.12	Other	arginase type II
Ccm2	0.50	0.44	2.18	Lethal	cerebral cavernous malformation 2
Cd72	0.06	0.15	2.52	Other	CD72 antigen
Cyp11a1	0.21	0.32	2.60	Lethal	cytochrome P450, family 11, subfamily a, polypeptide 1
Cyp2s1	0.06	0.11	16.51	Normal	cytochrome P450, family 2, subfamily s, polypeptide 1
Fblim1	0.27	0.50	2.44	Other	filamin binding LIM protein 1
Fgf16	0.18	0.34	3.69	Lethal	fibroblast growth factor 16
Fibcd1	0.44	0.28	2.00	ND	fibrinogen C domain containing 1
Gls2	0.28	0.44	3.09	ND	glutaminase 2 (liver, mitochondrial)
Gpr139	0.27	0.12	3.80	Other	G protein-coupled receptor 139
Hr	0.45	0.38	3.72	Other	Hairless, lysine demethylase and nuclear receptor corepressor
Il17rc	0.21	0.36	2.51	Other	interleukin 17 receptor C
Kctd17	0.33	0.35	2.91	Other	potassium channel tetramerisation domain containing 17
Lpcat4	0.39	0.42	2.25	Other	lysophosphatidylcholine acyltransferase 4
Lynx1	0.46	0.30	2.00	Neural Phenotype	Ly6/neurotoxin 1
Me2	0.38	0.37	2.15	Other	malic enzyme 2, NAD(+)-dependent, mitochondrial
Mme	0.13	0.33	2.50	Neural Phenotype	membrane metallo endopeptidase
Nrgn	0.24	0.32	2.39	Neural Phenotype	neurogranin
Nrtn	0.29	0.44	2.89	Other	neurturin
Pld5	0.38	0.33	2.35	Normal	phospholipase D family, member 5
Rasd2	0.40	0.39	2.32	Neural Phenotype	RASD family, member 2
Robo3	0.13	0.05	9.99	Neural Phenotype	roundabout guidance receptor 3
Sema7a	0.19	0.28	2.30	Neural Phenotype	sema domain, immunoglobulin domain (Ig), and GPI membrane anchor,
Sgpp2	0.16	0.15	3.18	Other	sphingosine-1-phosphate phosphotase 2

Table S5 (continued).

	FC *Thra*$^{AMI/gn}$	FC hypoth.	FC TH response	KO mouse phenotype	Full name
Shh	0.29	0.39	2.52	Neural Phenotype	sonic hedgehog
Slc22a3	0.35	0.34	2.13	Neural Phenotype	solute carrier family 22 (organic cation transporter), member 3
Slc26a10	0.22	0.31	2.40	Neural Phenotype	solute carrier family 26, member 10
Slc38a8	0.38	0.30	2.73	ND	solute carrier family 38, member 8
Slc41a1	0.45	0.39	2.12	ND	solute carrier family 41, member 1
Smpd3	0.44	0.48	2.02	Other	sphingomyelin phosphodiesterase 3,
Tbc1d10c	0.42	0.39	2.26	Other	TBC1 domain family, member 10c
Ubash3b	0.40	0.49	2.08	Normal	ubiquitin associated and SH3 domain

Transparent methods

Mouse models and treatments

All experiments were carried out in accordance with the European Community Council Directive of September 22, 2010 (2010/63/EU) regarding the protection of animals used for experimental and other scientific purposes. The research project was approved by a local animal care and use committee (C2EA015) and subsequently authorized by the French Ministry of Research. Mice were bred and maintained at the Plateau de Biologie Expérimentale de la Souris (SFR BioSciences Gerland - Lyon Sud, France). Mice of either sex were used in all experiments. Whenever the influence of the age of the animals on the observed parameters was analyzed, we did not find any significant difference between males and females, which is congruent with the current literature on the role of thyroid hormone in mouse brain development. We indeed confirmed the absence of interaction between sex and thyroid hormone signaling at the genome-wide scale in our RNAseq analysis: differential gene expression analysis showed no effect of sex, except for 3 genes which are on the Y chromosome and thus expressed at low levels only in males. As our experiments were carried out using all mice from each litter, there was no bias in the sex of the animals: approximately half of them were males and half of them were females, but the male:female ratio in a given experiment was not necessarily harmonized between groups, since the sex was not considered as an influent parameter.

In order to target the expression of mutated forms of TRα1 specifically in GABAergic neurons, we used the Cre/loxP system with *Gad2Cre* mice (IMSR Cat# JAX:010802, RRID: IMSR_JAX:010802), which carry a Cre coding cassette immediately after the translation stop codon of the *Gad2* gene. In *Gad2Cre* mice, Cre recombinase expression is almost entirely restricted to GABAergic neurons and includes almost all GABAergic neurons (Taniguchi et al., 2011). *Gad2Cre* mice were crossed with $Thra^{AMI/+}$ (Quignodon et al., 2007) or $Thra^{Slox/+}$ (Markossian et al., 2018) mice, which carry mutated versions of the *Thra* gene preceded with a

floxed STOP cassette (Fig. 1). When indicated, a *Rosa26tdTomato* reporter transgene (also known as *Ai9,* MGI Cat# 4436851, RRID: MGI:4436851) was also included (Madisen et al., 2010). Finally, in order to address chromatin occupancy by TRα1 specifically in GABAergic neurons, we generated *ad hoc* $Thra^{TAG/gn}$ transgenic mice, which express a "tagged" receptor, $TR\alpha1^{TAG}$, only in GABAergic neurons (Fig. 1).

In order to compare the expression levels of mutant and wild-type *Thra* alleles, we evaluated peak surfaces after Sanger sequencing, using ICE software for quantification (Synthego, https://www.synthego.com/products/bioinformatics/crispr-analysis, see also : https://www.biorxiv.org/content/10.1101/251082v1) and genomic DNA for calibration.

In order to compare animals with different thyroid statuses, TH deficiency was induced in pups by giving a diet containing propylthiouracil (TD95125; Harlan Teklad) to dams from post-natal day 0 (PND0) to post-natal day 21 (PND 21). In half of hypothyroid pups, TH levels were restored by two intraperitoneal injections of a mixture of T4 (2g/kg) and T3 (0.2g/kg) given at PND19 and PND20.

Brain collection

For neuroanatomy experiments, each mouse was given a lethal intraperitoneal injection (6 mL/kg) of a mixture of ketamine (33 mg/mL) and xylazine (6.7 mg/mL). The thorax was opened and each mouse was perfused with 4% paraformaldehyde in 0.1M phosphate buffer at room temperature. Each brain was dissected out, immersed in fixative at 4°C for 3 hours and then in phosphate buffered saline (PBS) at 4°C until sectioning. Coronal sections (50 µm) were cut with the aid of a vibrating microtome (Integraslice 7550 SPDS, Campden Instruments, Loughborough, UK), in PBS at room temperature. Brain sections were stored at –20°C in cryoprotectant (30% ethylene glycol and 20% glycerol in 10 mM PBS) prior to immunohistochemistry. For transcriptome analyses, pups were killed by decapitation. The striatum was dissected out, snap frozen in either dry ice or liquid nitrogen and stored at –80°C prior to analysis. For Chip-Seq experiments, the

tissue was dissociated immediately after dissection and DNA-protein complexes were cross-linked by incubation in 1% formaldehyde for 20 min.

Brain histology

Immunohistochemistry was performed on free-floating brain sections. The following primary antibodies were used: mouse anti-parvalbumin (Sigma P3088, 1:2000), rabbit anti-NPY (Sigma N6528, 1:5000), goat anti-somatostatin (Clinisciences D20 sc-7819, 1:500) and mouse anti-calretinin (Swant 6B3, 1:1000). Secondary antibodies were made in donkey (anti-rabbit, anti-goat and anti-mouse DyLight 488, ThermoFisher Scientific) and used at a 1:1000 dilution. Antibodies were diluted in PBS with 0.2% Triton X-100, 1% normal donkey serum, 1% cold water fish skin gelatin and 1% dimethyl sulfoxide. Non-specific binding sites were blocked by incubating sections for 1 h in PBS with 10% normal donkey serum, 1% cold water fish skin gelatin and 0.2% Triton X-100. Primary antibody incubation was carried out overnight at 4°C and sections were washed in PBS with 1% normal donkey serum and 1% cold water fish skin gelatin. Sections were further incubated for 10 min at room temperature with DAPI (4',6-diamidino-2-phenylindole, 1:5000, Sigma). Incubation with the secondary antibodies lasted for 3h at room temperature. Sections were mounted in FluoroshieldTM (Sigma), coverslipped and imaged using an inverted confocal microscope (Zeiss LSM 780).

In order to label perineuronal nets, sections were incubated with biotinylated *Wisteria floribunda* lectin (WFL, Vector Laboratories B-1355, 20 µg/mL) overnight at 4°C, followed by incubating with DyLight488 streptavidin (Vector Laboratories, SA-5488, 1:1000). Sections were washed with PBS. WFL and fluorescent streptavidin were diluted in PBS with 0.2% Triton X-100, 1% bovine serum albumine and 1% dimethyl sulfoxide.

Transcriptome analysis

RNA was extracted from the striatum using a Macherey-Nagel NucleoSpin RNA II kit. RNAseq was used to compare gene expression levels between control mice (n=4), hypothyroid mice (n=5) and hypothyroid mice treated for 48 hours with T4 and T3 (n=5). cDNA libraries were prepared

using the total RNA SENSE kit (Lexogen, Vienna Austria) and analyzed on an Ion Proton sequencer (Thermofisher, Waltham MA, USA). Comparison of the striatal transcriptome between *Thra*$^{AMI/gn}$ mice and wild-type littermates was performed at PND7 and PND14 using the Ion AmpliSeq™ Transcriptome Mouse Gene Expression Kit (Thermofisher, Waltham MA, USA). All libraries were sequenced (> 10^7 reads/library) on an Ion Proton sequencer (Thermofisher, Waltham MA, USA). For RNAseq, a count table was prepared using htseq-count (Galaxy Version 0.6.1galaxy3) (Anders et al., 2015). Differential gene expression analysis was performed with DEseq2 (Galaxy Version 2.1.8.3) (Love et al., 2014) using the following thresholds: FDR < 0.05; p-adjusted value < 0.05; expression > 10 reads per million. We used both one factor analysis, in striatum, or 2 factors analysis (genotype and age of mice for cortex) to maximize the number of differentially expressed genes. A supplementary threshold (fold-change >2 or <0.5) was used for striatum. Hierarchical clustering was performed using the Cluster 3.0 R package (Euclidian distance, Ward's algorithm).

Chromatin occupancy by GS-TRα1

Chromatin immunoprecipitation for Chip-Seq analysis was performed as previously described (16). As a quality control, quantitative PCR was used to confirm enrichment of known TR binding sites (*Klf9* gene, chr19:23135795-23136233, 4.96% of input. Primer sequences: TGCACGAGTTTGGGGCGGATTC (Forward) and TGGGCCTGGCATCGCCCTTTTA (Reverse)) compared to control sequences located within 1kb on the same chromosome (<1% input. Primer sequences: CACGGGAAAGGCTGGGTTGTGA (Forward) and TTACTGTCTCTACCTCTGGGCCTGC (Reverse)). Libraries were prepared from the immunoprecipitated fraction and the input fraction as control, and sequenced on Ion Proton (Thermoscientific). 27.10^6 reads were obtained for each library. Reads were mapped on the mouse genome (GRCm38/mm10 version) using Bowtie2 (Galaxy Version 2.3.4.2). MACS2 (Galaxy Version 2.1.1.20160309.0) was used for peak calling. Peaks with a score inferior to 60 were filtered out, as well as peaks overlapping the "blacklist" of common artefacts (https://www.encodeproject.org/annotations/ENCSR636HFF/). *De novo* motif search was performed using MEME-ChIP (Machanick and Bailey, 2011). We chose a distance of

30kb upstream or downstream of the transcription start site to attribute a TRBS to a gene. Although arbitrary, this distance was found to maximize the ratio of T3-responsive genes among the included genes, without excluding genes which have been well characterized as TRα1 target genes in other neural systems, such as *Klf9* or *Hr* (Gil-Ibanez et al., 2015).

q-RT-PCR

Striatum samples from 2-week old mice of either sex were dissected out, snap frozen and kept at −80◦C until RNA extraction. Total RNA was extracted using RNeasy Mini kit (Qiagen). RNA concentrations were measured with a Nanodrop spectrophotometer (ThermoScientific) and 1 µg of each RNA sample was reverse transcribed in murine leukemia virus reverse transcriptase (Promega) and random DNA hexamer primers. Quantitative PCR was performed according to a standard protocol, using the Biorad iQ SYBRGreen kit and the Biorad CFX96thermocycler. *Hprt*, a housekeeping gene, was used as internal control. For each pair of primers (Table S4), a standard curve was established and PCR efficiency was controlled to be within usable range (90%–110%) before analysis using the $2^{-D\Delta(Ct)}$ method (Livak and Schmittgen, 2001).

Statistical analysis

The density of immunoreactive neurons, the intensity of immunofluorescence and the expression level of genes (qPCR data) of mutant mice were systematically analyzed as a fraction of the corresponding values observed in control littermates. Group means were subsequently compared between mutant and control mice using unpaired *t*-tests.

Data and software availability

RNASeq and ChipSeq data are accessible through GEO Series accession number GSE143933 (https://www.ncbi.nlm.nih.gov/geo/query/acc.cgi?acc=GSE143933).

References for supplemental information

Anders, S., Pyl, P.T. and Huber, W. (2015). HTSeq--a Python framework to work with high-throughput sequencing data. *Bioinformatics,* 31**,** 166-9.

Gil-Ibañez, P., Garcia-Garcia, F., Dopazo, J., Bernal, J. and Morte, B. (2015). Global Transcriptome Analysis of Primary Cerebrocortical Cells: Identification of Genes Regulated by Triiodothyronine in Specific Cell Types. *Cereb Cortex***,** 1-12.

Livak, J.L. and Schmittgen, T.D. (2001). Analysis of relative gene expression data using real-time quantitative PCR and the 2-DDCT method. *Methods,* 25**,** 402-408.

Love, M.I., Huber, W. and Anders, S. (2014). Moderated estimation of fold change and dispersion for RNA-seq data with DESeq2. *Genome Biol,* 15**,** 550.

Machanick, P. and Bailey, T.L. (2011). MEME-ChIP: motif analysis of large DNA datasets. *Bioinformatics,* 27**,** 1696-7.

Madisen, L., Zwingman, T.A., Sunkin, S.M., Oh, S.W., Zariwala, H.A., Gu, H., Ng, L.L., Palmiter, R. D., Hawrylycz, M.J., Jones, A.R., Lein, E.S. and Zeng, H. (2010). A robust and high-throughput Cre reporting and characterization system for the whole mouse brain. *Nat Neurosci,* 13**,** 133-40.

Markossian, S., Guyot, R., Richard, S., Teixeira, M., Aguilera, N., Bouchet, M., Plateroti, M., Guan, W., Gauthier, K., Aubert, D. and Flamant, F. (2018). CRISPR/Cas9 Editing of the Mouse Thra Gene Produces Models with Variable Resistance to Thyroid Hormone. *Thyroid,* 28**,** 139-150.

Quignodon, L., Vincent, S., Winter, H., Samarut, J. and Flamant, F. (2007). A point mutation in the activation function 2 domain of thyroid hormone receptor alpha1 expressed after CRE-mediated recombination partially recapitulates hypothyroidism. *Mol Endocrinol,* 21**,** 2350-60.

Taniguchi, H., He, M., Wu, P., Kim, S., Paik, R., Sugino, K., Kvitsiani, D., Fu, Y., Lu, J., Lin, Y., Miyoshi, G., Shima, Y., Fishell, G., Nelson, S. B.and Huang, Z. J. (2011). A resource of Cre driver lines for genetic targeting of GABAergic neurons in cerebral cortex. *Neuron,* 71**,** 995-1013.